Predictive Control for Autonomous Driving With Uncertain, Multimodal Predictions

Siddharth H. Nair, Hotae Lee, *Member, IEEE*, Eunhyek Joa, *Member, IEEE*, Yan Wang, H. Eric Tseng, and Francesco Borrelli, *Fellow, IEEE*

***Abstract*— We propose a stochastic model predictive control (SMPC) formulation for path planning with autonomous vehicles in scenarios involving multiple agents with multimodal predictions. The multimodal predictions capture the uncertainty of urban driving in distinct modes/maneuvers (e.g., yield and keep speed) and driving trajectories (e.g., speed and turning radius), which are incorporated for multimodal collision avoidance chance constraints for path planning. In the presence of multimodal uncertainties, it is challenging to reliably compute feasible path planning solutions at real-time frequencies (≥10 Hz). Our main technological contribution is a convex SMPC formulation that simultaneously 1) optimizes over parameterized feedback policies and 2) allocates risk levels for each mode of the prediction. The use of feedback policies and risk allocation enhances the feasibility and performance of the SMPC formulation against multimodal predictions with large uncertainty. We evaluate our approach via simulations and road experiments with a full-scale vehicle interacting in closed loop with virtual vehicles. We consider distinct, multimodal driving scenarios: 1) negotiating a traffic light (TL) and a fast, tailgating agent; 2) executing an unprotected left turn at a traffic intersection; and 3) changing lanes in the presence of multiple agents. For all these scenarios, our approach reliably computes multimodal solutions to the path-planning problem at real-time frequencies.**

***Index Terms*— Autonomous driving, mixture models, predictive control, uncertain systems.**

I. Introduction

A. Motivation

AUTONOMOUS vehicle technologies have seen a surge in popularity over the last decade, with the potential to improve the flow of traffic, safety, and fuel efficiency [1]. In the upcoming decade, we can expect a rise in the number of autonomous vehicles, making it increasingly common for them to navigate roads with mixed traffic with vehicles of varying automation levels [2]. While the existing technology is being gradually introduced into scenarios such as highway driving [3] and low-speed parking [4] where other road users' intents are relatively easy to infer, autonomous driving in mixed traffic scenarios such as urban road driving and merging is an open challenge because of the variability in the possible behaviors of the surrounding agents [5], [6]. To address this difficulty, significant research has been devoted to modeling these agent predictions as multimodal distributions [7], [8], [9]. Such models capture uncertainty in both high-level decisions (desired route) and low-level executions (agent position, heading, and speed).

The focus of this work is to incorporate these multimodal distributions for the surrounding agents [called target vehicles (TVs)] into a planning framework for the autonomous agent [called ego vehicle (EV)]. We investigate the planning problem in the context of constrained optimal control and use model predictive control (MPC) for computing feedback control policies. The main challenge in designing MPC for effectively addressing the multimodal predictions is to find a good balance among *performance*, *safety*, and *computational efficiency*. Consider the situation in Fig. 1(a), where the EV is approaching a traffic light (TL) with a tailgating TV behind. A *performant* MPC design would enable the EV to assess the risk associated with the multimodalities of the TV and TL along the planning horizon so that the EV is able to cross the yellow light or stop at the red light. For ensuring *safety*, the EV must also manage a safe distance ahead of the TV despite the uncertain predictions. A conservative MPC design would either fail to find a feasible solution in the presence of large uncertainty, or sacrifice performance for safety by always choosing to stop. Prior works [10], [11], [12], [13], [14] show that planning using trees or feedback policies over the multimodal distribution is effective for reliably finding high-quality solutions. However, optimization over policies is infinite-dimensional in general and hence, *computationally expensive* for real-time control. In this work, we propose a stochastic MPC (SMPC) framework that incorporates multimodal predictions of agents to enforce probabilistic collision avoidance and state-input constraints.

B. Contributions

Our main contributions are summarized as follows. First, we propose a convex formulation for SMPC that optimizes over tree-structured feedback policies for multimodal predictions specified as Gaussian mixture models (GMMs). The policy parameterization is designed to receive feedback over

Manuscript received 31 October 2023; revised 3 November 2023 and 2 May 2024; accepted 29 July 2024. Date of publication 17 September 2024; date of current version 26 June 2025. This work was supported in part by Ford Research Laboratories and Advanced Research Projects Agency–Energy (ARPA-E), U.S. Department of Energy, under Grant DE-AR0000791. Recommended by Associate Editor J. Tumova. *(Siddharth H. Nair, Hotae Lee, and Eunhyek Joa contributed equally to this work.) (Corresponding author: Siddharth H. Nair.)*

Siddharth H. Nair, Hotae Lee, Eunhyek Joa, and Francesco Borrelli are with the Model Predictive Control Laboratory, University of California, Berkeley, Berkeley, CA 94720 USA (e-mail: siddharth_nair@berkeley.edu; hotae.lee@berkeley.edu; e.joa@berkeley.edu; fborrelli@berkeley.edu).

Yan Wang is with Ford Research and Advanced Engineering, Dearborn, MI 48124 USA.

H. Eric Tseng is with the University of Texas at Arlington, Arlington, TX 76109 USA (e-mail: hongtei.tseng@uta.edu).

Digital Object Identifier 10.1109/TCST.2024.3451370

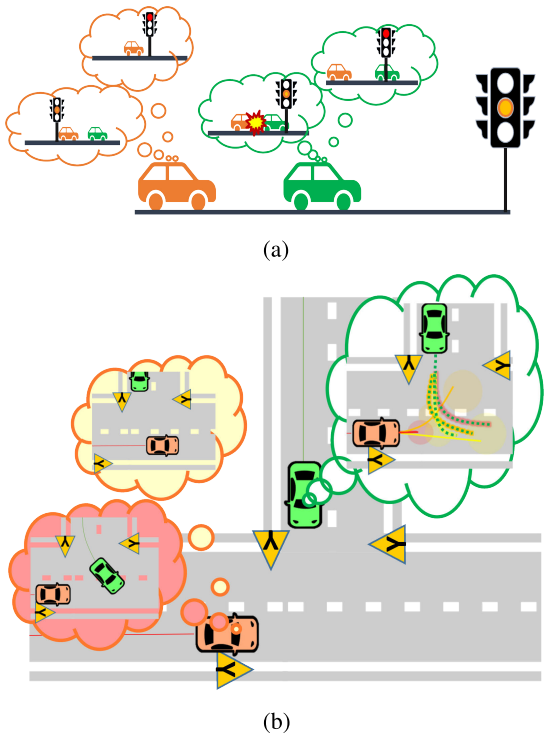

Fig. 1. Multimodal planning in urban driving. (a) EV (green) must decide whether to cross a TL before it turns red or comes to a stop, while managing the headway for the tailgating TV behind. The discrete modes are given as {TL goes red, TL stays yellow} × {TV stops for TL, TV doesn't stop for TL}. Inspired by the dashcam footage: https://youtu.be/i3pvrpKDjRQ. (b) EV (green) must find a feasible solution to make a left turn in the presence of an oncoming TV while accounting for its multimodal behavior: {give EV right-of-way, go straight, and turn left}. The EV computes a *policy tree* to address the multimodal uncertainty. Inspired by the footage: https://shorturl.at/aeJ12.

both discrete modes and continuous observations of the TVs' states. Our formulation also includes a novel multimodal chance constraint reformulation that simultaneously allocates risk levels for the various modes based on their probabilities. Second, we evaluate our approach in various autonomous driving scenarios via simulations and hardware experiments. We demonstrate our SMPC via a hardware experiment for a lane change (LC) scenario, characterized by the presence of two TVs with uncertain, bimodal predictions. Our findings indicate that the proposed approach exhibits a significant reduction in conservatism when compared to the conventional approaches that optimize over open-loop (OL) control sequences. Additionally, we show adaptability to variable probabilities of the modes of the TVs.

C. Related Work

There is a large body of work focusing on the application of SMPC to autonomous driving for motion planning [15], [16], [17]. A typical SMPC algorithm involves a finite-horizon stochastic optimal control problem that is solved as a chance-constrained optimization problem in receding horizon fashion [18]. In the context of motion planning, SMPC has been used for imposing chance-constrained collision avoidance to account for uncertainty in vehicles' predictions in applications such as autonomous LC [19], [20], cruise control [21], and platooning [22]. Besides the modeling aspects specific to the applications, SMPC formulations differ in the uncertainty descriptions and the deterministic reformulations of the chance constraints. Gaussian distributions are a common modeling choice for the uncertainty owing to the invariance to affine transformations and closed-form expressions for affine chance constraints [16], [23]. For arbitrary distributions that can be sampled efficiently, randomized approaches [24] are used to obtain high-confidence reformulations of the chance constraints [25]. Distributionally robust formulations are also becoming increasingly popular to improve robustness to distributional assumptions [26], [27], [28], by robustifying the chance constraint against a set of distributions. For urban driving scenarios where the surrounding agents' predictions are multimodal and temporally linked, mixture models [29], [30], [31], [32], [33] and scenario trees [10], [11], [34] offer convenient structure that can be exploited in the SMPC.

To enhance the feasibility of the SMPC optimization problem, the scenario-tree-based MPC formulations [10], [11], [34] optimize over policies along the prediction horizon. The policies inherit a tree structure from the scenario tree, to encode feedback over the uncertainty realization. This adds flexibility to find feasible solutions due to the ability to react to different realizations of the vehicles' trajectory predictions along the prediction horizon. Mixture models like GMMs are more memory-efficient representations for the multimodal uncertainty by using discrete random variables to capture distinct modalities and continuous variables to capture the spread within each mode. In order to handle multimodal predictions (specifically GMMs), Zhou et al. [29] and Wang et al. [30] propose nonlinear SMPC algorithms that suitably reformulate the collision avoidance chance constraint for all possible modes. However, a nonconvex optimization problem is formulated to find a single OL input sequence that satisfies the collision avoidance chance constraints for all modes and possible evolutions of the TVs over the prediction horizon given by the GMM. To remedy the conservativism of this approach, we proposed a convex SMPC formulation [12] that optimizes over a parametric, mixed-feedback policy architecture to enhance the feasibility of the SMPC optimization problem. Inspired by scenario trees, our policies use feedback from the discrete mode realization but also incorporate feedback from the continuous realizations of the agents' positions.

In this work, we build on our SMPC formulation [12] in two directions. First, we generalize our policy parameterization for multimodal predictions with arbitrary rooted tree structure. Our earlier approach assumed a simplistic tree structure with a single branching point. Second, we derive a convex reformulation of the multimodal chance constraints to simultaneously allocate risk levels for each mode and find feasible policy parameters. Compared to our previous approach, this further enhances the feasibility of the SMPC optimization problem by exploiting the varying probabilities of the discrete modes to allocate risk levels for each mode to satisfy the multimodal chance constraint. In the context of SMPC, risk allocation has been studied for joint chance constraints [35], [36]. In [35], the risk levels are iteratively optimized by alternating optimization of risk levels and SMPC

optimal control problem, whereas Sivaramakrishnan et al. [36] propose a convex formulation for simultaneous risk allocation and optimization over OL control sequences. The simultaneous optimization in [36] overcomes the computational overhead of the iterative optimization approach for real-time applications, but is not applicable when the SMPC optimizes over policies.

Multiple works dealing with multitraffic scenarios are investigated in simulation settings [10], [16], [34], [37]. Validating developed autonomous vehicle technology through vehicle tests is desirable to demonstrate its capabilities and effectiveness in real-world setups. However, investigating algorithms in real-world multitraffic scenarios is challenging due to safety concerns and legal issues. In order to mitigate these challenges associated with evaluating the performance of the proposed control system, a vehicle-in-the-loop (VIL) setup is adopted [38], [39]. In the VIL setup, the EV is driven in the real world, in closed loop with the proposed control algorithm while interacting with virtual surrounding vehicles which are simulated using a microscopic simulator [40], [41]. This allows us to test the performance of the proposed control system in a more realistic yet safe environment, while still leveraging the benefits of simulation for perception and driving environment construction.

II. Problem Formulation

In this section, we formally cast the problem of designing SMPC in the context of autonomous driving.

A. Preliminaries

1) Notation: The index set $\{k_1, k_1+1, \ldots, k_2\}$ is denoted by $\mathbb{I}_{k_1}^{k_2}$. The cardinality of a discrete set $\mathcal{S}$ is denoted by $|\mathcal{S}|$ (e.g., $|\mathbb{I}_{k_1}^{k_2}| = k_2 - k_1 + 1$). We denote $\|\cdot\|$ by the Euclidean norm and $\|x\|_M = \|\sqrt{M}x\|$ for some $M \succ 0$. The binary operator $\otimes$ denotes the Kronecker product. The partial derivative of function $f(x,u)$ with respect to x at $(x,u) = (x_0,u_0)$ is denoted by $\partial_x f(x_0,u_0)$.

2) EV Modeling: We model the dynamics of the EV in the Frenet frame moving along a curve $\gamma(s) = [\bar{X}(s), \bar{Y}(s), \bar{\psi}(s)]$ parameterized by the arc length s, which describes the position and heading of the centerline of a lane in the road [42]. Let $x_t = [s_t,\ e_{y,t},\ e_{\psi,t},\ v_t]^\top$ be the state of the EV at time t, where $s_t, e_{y,t}, and e_{\psi,t}$ are the arc length, lateral offset, and relative heading with respect to the centerline $\gamma(\cdot)$, and v_t is the EV's speed. Then the dynamics of the EV can be described as follows:

$$\dot{x}_t = \begin{bmatrix} \dfrac{v_t \cos(e_{\psi,t})}{1 - e_{y,t}\kappa(s_t)} \\ v_t \sin(e_{\psi,t}) \\ \dot{\psi}_t - \dfrac{v_t \cos(e_{\psi,t})\kappa(s_t)}{1 - e_{y,t}\kappa(s_t)} \\ a_t \end{bmatrix} \tag{1}$$

where $\kappa(s_t) = ((d\bar{\psi}(s_t))/ds)$ describes the curvature of $\gamma(\cdot)$, a_t is the EV's acceleration, and $\dot{\psi}_t$ is the EV's global yaw rate. The dynamics of the EV are time-discretized (with any explicit integration scheme) to obtain the model $x_{t+1} = f^{\mathrm{EV}}(x_t, u_t)$, with inputs $u_t = [a_t,\ \dot{\psi}_t]$. Given the state x_t, the EV's global pose can be obtained via a function $\mathcal{G}^\gamma(\cdot)$

$$\begin{bmatrix} X_t \\ Y_t \\ \psi_t \end{bmatrix} = \mathcal{G}^\gamma(x_t) = \begin{bmatrix} \bar{X}(s_t) - e_{y,t}\sin(\bar{\psi}(s_t)) \\ \bar{Y}(s_t) + e_{y,t}\cos(\bar{\psi}(s_t)) \\ e_{\psi,t} + \bar{\psi}(s_t) \end{bmatrix}. \tag{2}$$

The system state and input constraints are given by polytopic sets which capture vehicle actuation limits and traffic rules

$$\begin{aligned} \mathcal{X} &= \left\{ x : a_{x,i}^\top x \le b_{x,i}, \forall i \in \mathbb{I}_1^{n_X} \right\} \\ \mathcal{U} &= \left\{ u : a_{u,i}^\top u \le b_{u,i}, \forall i \in \mathbb{I}_1^{n_U} \right\}. \end{aligned} \tag{3}$$

We assume that a kinematically feasible reference trajectory

$$\left\{ \left(x_t^{\mathrm{ref}}, u_t^{\mathrm{ref}} \right) \right\}_{t=0}^{T} \tag{4}$$

is provided for the EV. This serves as the EV's desired trajectory which can be computed offline (or online at lower frequency) accounting for the EV's route, actuation limits, and static environment constraints (like lane boundaries and traffic rules). However, this reference does not consider the dynamically evolving TVs for real-time obstacle avoidance.

3) TV Predictions: Let n_{TV} be the number of TVs in consideration and denote the position of the ith TV at time t as $o_t^i = [X_t^i\ Y_t^i]^\top$, and define $o_t = [o_t^{1\top}, \ldots, o_t^{n_{\mathrm{TV}}\top}]^\top$ which stacks the positions of all the TVs. For collision avoidance, we use an off-the-shelf prediction model [8], [9] trained on traffic datasets [43], [44] that provides N-step predictions of the TVs' positions given by a multimodal linear time-varying (LTV) model $\forall k \in \mathbb{I}_t^{t+N}$, $j \in \mathbb{I}_1^J$

$$o_{k+1|t,j} = T_{k|t,j} o_{k|t,j} + c_{k|t,j} + n_{k|t,j} \tag{5}$$

where $o_{k|t,j}$ is the prediction of the TVs' positions at time k for mode j, $T_{k|t,j}, c_{k|t,j}$ are the time-varying matrices and vectors for the TVs' prediction for mode j, and the process noise is given by $n_{k|t,j} \sim \mathcal{N}(0, \Sigma_{k|t,j})$. The mode $j \in \mathbb{I}_1^J$ captures distinct interactions/maneuvers of the TVs as a group. Note that if multimodal predictions are made for each TV separately, then $J = P^{n_{\mathrm{TV}}}$, where P is the number of modes predicted for each TV. We denote $p_t = [p_{t,1}, \ldots, p_{t,J}]$ as the probability distribution over the modes at time t, and σ_t to be the true, *unknown* mode.

B. SMPC Formulation

We aim to design a computationally efficient feedback control $u_t = \pi_t(x_t, o_t)$ for the EV to track the reference trajectory (4), satisfy state-input constraints, and avoid collisions with the TVs by effectively addressing the uncertainty arising from the TVs' multimodal predictions (5).

We propose an SMPC formulation to compute the feedback control u_t. The optimization problem of our SMPC takes the form

$$\min_{\{\theta_{t,j}\}_{j=1}^J} \sum_{j=1}^{J} p_{t,j} \mathbb{E}\left[C_t(\mathbf{x}_{t,j}, \mathbf{u}_{t,j}) \right] \tag{6a}$$

$$\text{s.t. } x_{k+1|t,j} = f_k^{\mathrm{EV}}(x_{k|t,j}, u_{k|t,j}) \tag{6b}$$

$$o_{k+1|t,j} = T_{k|t,j} o_{k|t,j} + c_{k|t,j} + n_{k|t,j} \tag{6c}$$

$$\sum_{j=1}^{J} p_{t,j} \mathbb{P}(g_k(x_{k+1|t,j}, o^i_{k+1|t,j}) < 0) \leq \epsilon \tag{6d}$$

$$(x_{k+1|t,j}, u_{k|t,j}) \in \mathcal{X} \times \mathcal{U} \tag{6e}$$

$$\mathbf{u}_{t,j} \in \Pi_{\theta_{t,j}}(\mathbf{x}_{t,j}, \mathbf{o}_{t,j}) \tag{6f}$$

$$x_{t|t,j} = x_t, \; u_{t|t,j} = u_{t|t,1}, \; o_{t|t,j} = o_t$$
$$\forall i \in \mathbb{I}_1^{n_{\mathrm{TV}}} \quad \forall j \in \mathbb{I}_1^J \; \forall k \in \mathbb{I}_t^{t+N-1} \tag{6g}$$

where $\mathbf{u}_{t,j} = [u_{t|t,j}, \ldots, u_{t+N-1|t,j}]$, $\mathbf{x}_{t,j} = [x_{t|t,j}, \ldots, x_{t+N|t,j}]$, and $\mathbf{o}_{t,j}$ (defined similarly to $\mathbf{x}_{t,j}$) denotes stacked predictions along the horizon for mode j. The problem (6) is formulated in the single-shooting/batch form [45] and the SMPC feedback control action is obtained from the optimal solution as follows: as follows:

$$u_t = \pi_{\mathrm{SMPC}}(x_t, o_t) = u^\star_{t|t,1} \tag{7}$$

where the EV and TV state feedback (SF) enters the optimization problem in (6g). The function $C_t(\cdot,\cdot)$ in the objective (6a) penalizes the deviation of the EV's trajectory for mode j from the reference (4), and is weighted by the probability of the mode given by $p_{t,j}$. The collision avoidance constraints are imposed as muti-modal chance constraints (6d) along with polytopic state and input constraints $\mathcal{X}, \mathcal{U}$ for the EV. The EV's controls along the prediction horizon are given by parameterized policies $\Pi_{\theta_{t,j}}(\mathbf{x}_{t,j}, \mathbf{o}_{t,j})$ (6f) that are functions of the EV's and TVs' states, as opposed to OL sequences, as depicted in Fig. 2. The policies are multimodal, which makes the EV's closed-loop trajectories in (6b) multimodal. Deriving a deterministic reformulation of the multimodal chance constraint (6d) that is computationally efficient, but not too conservative is the key technical challenge in the SMPC design. Toward addressing this challenge, our SMPC formulation features the following: 1) a novel multimodal policy parameterization (6f) for shaping the multimodal closed-loop distribution; 2) a convex inner approximation technique for the multimodal chance constraint (6d) involving mode-dependent risk levels $r_{t,j} = 1 - \epsilon_{t,j}$ for $\epsilon_{t,j} \in [0, 1]$; and 3) simultaneous, convex optimization over policy parameters and risk levels for control computation. These features enable computationally efficient synthesis of (7) while enhancing the feasibility of (6) by effectively addressing the multimodal uncertainty.

III. SMPC With Multimodal Predictions

In this section, we detail our SMPC formulation for the EV to track the reference (4) while incorporating multimodal predictions (5) of the TV for obstacle avoidance.

A. Vehicles' Prediction Models

The EV prediction model (6b) is a LTV model, obtained by linearizing $f^{\mathrm{EV}}(\cdot)$ about the reference trajectory (4). At time t, let $\bar{t} = -t + \arg\min_{k \in \mathbb{I}_0^T} |s_t - s_k^{\mathrm{ref}}|$ and define $\Delta x_{k|t} = x_{k|t} - x^{\mathrm{ref}}_{k+\bar{t}}$ and $\Delta u_{k|t} = u_{k|t} - u^{\mathrm{ref}}_{k+\bar{t}}, \forall k \in \mathbb{I}_t^{t+N-1}$. Then the LTV model is given as follows:

$$\Delta x_{k+1|t} = A_{k|t} \Delta x_{k|t} + B_{k|t} \Delta u_{k|t} + w_{k|t}$$

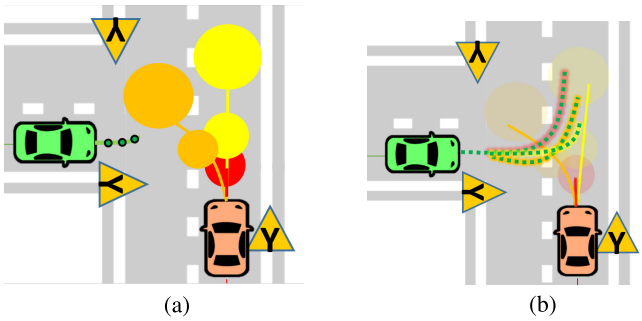

Fig. 2. (a) Solving (6) over OL sequences can be conservative because EV prediction (green-dashed) from a single sequence of control inputs must satisfy all the obstacle avoidance constraints. (b) Optimizing over policies (6f) allows for different EV predictions depending on the TV trajectory realizations (green-dashed with highlights corresponding to different TV trajectories).

$$A_{k|t} = \partial_x f^{\mathrm{EV}}(x^{\mathrm{ref}}_{k+\bar{t}}, u^{\mathrm{ref}}_{k+\bar{t}}), \quad B_{k|t} = \partial_u f^{\mathrm{EV}}\left(x^{\mathrm{ref}}_{k+\bar{t}}, u^{\mathrm{ref}}_{k+\bar{t}}\right) \tag{8}$$

where the additive process noise $w_{k|t} \sim \mathcal{N}(0, \Sigma_w)$ (i.i.d with respect to k) models linearization error and other stochastic noise sources. The polytopic state and input constraints (6e) are replaced by the chance constraints $\forall k \in \mathbb{I}_0^{N-1}$

$$\mathbb{P}((\Delta x_{k+1|t}, \Delta u_{k|t}) \in \Delta\mathcal{X}_k \times \Delta\mathcal{U}_k) \geq 1 - \epsilon$$
$$\Delta\mathcal{X}_k = \left\{\Delta x : a_{x,i}^\top \Delta x \leq b_{x,i} - a_{x,i}^\top x^{\mathrm{ref}}_{\bar{t}+k}, \forall \in \mathbb{I}_1^{n_X}\right\}$$
$$\Delta\mathcal{U}_k = \left\{\Delta u : a_{u,i}^\top \Delta x \leq b_{u,i} - a_{u,i}^\top u^{\mathrm{ref}}_{\bar{t}+k}, \forall \in \mathbb{I}_1^{n_U}\right\}. \tag{9}$$

B. Parameterized EV and TV SF Policies

We propose to use parameterized polices $\Pi_{\theta_t}(\mathbf{x}_t, \mathbf{o}_t)$ so that the EV's control $\mathbf{u}_t$ is a function of the EV and TV trajectories $\mathbf{x}_t, \mathbf{o}_t$ along the prediction horizon (as depicted in Fig. 2). Given the EV model (8) and mode-dependent TV model (5), consider the following feedback policy $\Delta u_{k|t,j} = \pi_{k|t,j}(x_{k|t,j}, o_{k|t,j})$ for the EV:

$$\Delta u_{k|t,j} = h^j_{k|t} + \sum_{l=t}^{k-1} M^j_{l,k|t} w_{l|t} + K^j_{k|t}(o_{k|t,j} - \mu_{k|t,j}) \tag{10}$$

where $\mu_{k|t,j} = \mathbb{E}[o_{k|t,j}]$ denotes the expected prediction of the TVs in (5). The variables $\{h^j_{k|t}, M^j_{l,k|t}, K^j_{k|t}\}$ *parameterize* the policy (10), and are decision variables in the SMPC optimization problem (20). The policy (10) uses SF for the TV states and affine disturbance feedback (ADF) for feedback over EV states. As shown in [46], the ADF $h^j_{k|t} + \sum_{l=0}^{k-1} M^j_{l,k|t} w_{l|t}$ is equivalent to SF $h^j_{k|t} + F^j_{k|t} \Delta x_{k|t,j}$, but the state prediction $\Delta x_{k|t,j}$ with ADF is affine in $\Delta x_{0|t,j}$ and the policy parameters up to time k $\{h_{s|t}, \{M_{l,s|t}\}_{l=0}^{s-1}\}_{s=0}^{k}$, whereas with SF, $\Delta x_{k|t}$ involves nonlinear products of the parameters $F_{k|t}, \ldots, F_{0|t}$. This is beneficial because the state predictions $\mathbf{x}_{t,j}$ become affine in the ADF policy parameters (at the cost of needing $O(N^2)$ parameters instead of $O(N)$ for SF).

SF policies for the TVs are beneficial toward scaling our approach to multiple TVs because we use $O(n_{\mathrm{TV}} \cdot N)$ parameters instead of $O(n_{\mathrm{TV}} \cdot N^2)$ parameters for ADF. Despite using SF for the TVs' states, $\Delta x_{k|t}$ are affine in $\{K_{s|t}\}_{s=0}^{k}$ $\forall k \in \mathbb{I}_0^{n-1}$

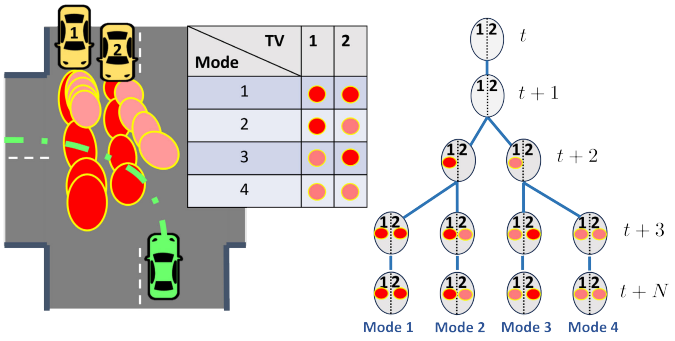

Fig. 3. Tree for encoding mode feedback along the prediction horizon. TV1's mode is revealed at time step $t+2$, whereas the TV2's mode is revealed at time $t+3$. Consequently, all the $J=4$ EV feedback policies share the same parameters in the interval $\mathbb{I}_t^{t+1}$. For time step $t+2$, parameters are shared by policies 1, 2 and 3, 4. After TV2's mode is revealed at time $t+3$, the $J=4$ policies have independent parameters in the interval $\mathbb{I}_{t+3}^{t+N}$. The policy constraints are described by the set $\mathcal{T}_t = \{(t+1,\{1,2\}),(t+1,\{1,3\}),(t+1,\{1,4\}),(t+2,\{1,2\}),(t+2,\{3,4\})\}$. The intervals for mode 4 are $\mathcal{B}_{t,4} = \{\mathbb{I}_t^{t+1}, \mathbb{I}_{t+2}^{t+2}, \mathbb{I}_{t+3}^{t+N}\}$.

as shown next. For mode $j \in \mathbb{I}_1^J$, define the stacked quantities along the prediction horizon $\Delta\mathbf{u}_{t,j}, \mathbf{w}_t, \mathbf{o}_{t,j}, \boldsymbol{\mu}_{t,j}$ (e.g., $\Delta\mathbf{u}_{t,j} = [\Delta u_{t|t,j}^\top, \ldots, \Delta u_{t+N-1|t,j}^\top]^\top$) and use (10) to get

$$\Delta\mathbf{u}_{t,j} = \mathbf{h}_t^j + \mathbf{M}_t^j \mathbf{w}_t + \mathbf{K}_t^j (\mathbf{o}_{t,j} - \boldsymbol{\mu}_{t,j})$$

using the stacked policy parameters $\mathbf{h}_t^j \in \mathbb{R}^{2N}, \mathbf{M}_t^j \in \mathbb{R}^{2N\times 4N}$, *and* $\mathbf{K}_t^j \in \mathbb{R}^{2N\times 2N\cdot n_{\mathrm{TV}}}$ [(22)–(24) in Appendix]. Denote the stacked EV closed-loop predictions for mode j as $\boldsymbol{\Delta x}_{t,j}$ and the TV's stacked process noise as $\mathbf{n}_{t,j}$. Using matrices $\mathbf{A}_t, \mathbf{B}_t, \mathbf{T}_t^j, \mathbf{C}_t^j, \mathbf{L}_t^j$, and $\mathbf{E}_t$ defined by (25) and (26) in the appendix, the closed-loop EV predictions are

$$\begin{aligned}\boldsymbol{\Delta x}_{t,j} &= \mathbf{A}_t \Delta x_{t|t} + \mathbf{B}_t(\mathbf{h}_t^j + \mathbf{K}_t^j(\mathbf{o}_{t,j} - \boldsymbol{\mu}_{t,j})) + (\mathbf{E}_t + \mathbf{B}_t\mathbf{M}_t^j)\mathbf{w}_t \\ &= \mathbf{A}_t \Delta x_{t|t} + \mathbf{B}_t(\mathbf{h}_t^j + \mathbf{K}_t^j\mathbf{L}_t^j\mathbf{n}_{t,j}) + (\mathbf{E}_t + \mathbf{B}_t\mathbf{M}_t^j)\mathbf{w}_t\end{aligned}$$

which are affine in $\mathbf{h}_t^j, \mathbf{M}_t^j$, and $\mathbf{K}_t^j$. The last equality uses $\boldsymbol{\mu}_{t,j} = \mathbb{E}[\mathbf{o}_{t,j}] = \mathbf{T}_t^j o_t + \mathbf{C}_t^j + \mathbf{L}_t^j \mathbf{n}_{t,j}$ from (26).

The policy parameters $\boldsymbol{\Theta}_t(x_t, o_t) = \{\mathbf{h}_t^j, \mathbf{M}_t^j, \mathbf{K}_t^j\}_{j=1}^J$ define J feedback policies $\Delta\mathbf{u}_{t,j} = \mathbf{h}_t^j + \mathbf{M}_t^j\mathbf{w}_t + \mathbf{K}_t^j\mathbf{o}_{t,j}$ that assume feedback from $\mathbf{x}_{t,j}$ and $\mathbf{o}_{t,j}$ along the prediction horizon and the mode $j \in \mathbb{I}_1^J$. To have J-independent feedback policies starting from times step $t+1$, the mode must be revealed at the time step $k = t+1$. To model more complex mode feedback information structures along the horizon, we use the notion of an information tree as illustrated in Fig. 3. Additional constraints imposed on $\boldsymbol{\Theta}_t(x_t, o_t)$ incorporate the mode feedback information structure along the prediction horizon, so that (20) optimizes over *realizable* policies. For example, if the EV optimizes for J different policies along the prediction horizon but the TVs' mode is revealed at time step $t+N-1$, then it is ambiguous whether which of the J policies the EV must use in the interval $\mathbb{I}_{t+1}^{t+N-2}$. In practice, the predictions (5) and control (7) are computed in a receding horizon fashion, but optimistically optimizing over unrealizable policies incurs infeasibilities when solving (6).

To formalize the constraints on $\boldsymbol{\Theta}_t(x_t, o_t)$, let the mode feedback information structure be defined by the set $\mathcal{T}_t \subset \mathbb{I}_t^{t+N} \times (\mathbb{I}_1^J \times \mathbb{I}_1^J)$, where $(k, \{j_1, j_2\}) \in \mathcal{T}_t$ corresponds to modes j_1 and j_2 being ambiguous in interval $\mathbb{I}_t^k$. Given $(k, \{j_1, j_2\}) \in \mathcal{T}_t$, we constrain the policy parameters of modes j_1 and j_2 as follows:

$$h_{k'|t}^{j_1}, K_{k'|t}^{j_1}, \left\{M_{l,k'|t}^{j_1}\right\}_{l=t}^{k'-1} = h_{k'|t}^{j_2}, K_{k'|t}^{j_2}, \left\{M_{l,k'|t}^{j_2}\right\}_{l=t}^{k'-1} \quad \forall k' \in \mathbb{I}_t^k$$

so that the policies of modes j_1 and j_2 are same up to time k. For the example in Fig. 3, the policy parameterization for mode $j=4$ and $N=4$ is given as follows:

$$\mathbf{h}_t^4 = \left[h_{t|t}^{1\top}\ h_{t+1|t}^{1\top}\ h_{t+2|t}^{3\top}, h_{t+3|t}^{4\top}, \ldots, h_{t+N-1|t}^{4\top}\right]^\top$$

$$\mathbf{K}_t^4 = \mathrm{blkdiag}\left(K_{t|t}^1, K_{t+1|t}^1, K_{t+2|t}^3, K_{t+3|t}^4, \ldots, K_{t+N-1|t}^4\right)$$

$$\mathbf{M}_t^4 = \begin{bmatrix} O & O & O & O \\ M_{t,t+1|t}^1 & O & O & O \\ M_{t,t+2|t}^3 & M_{t+1,t+2|t}^3 & O & O \\ M_{t,t+3|t}^4 & M_{t+1,t+3|t}^4 & M_{t+2,t+3|t}^4 & O \end{bmatrix}.$$

For each mode j, we denote $\mathcal{B}_{t,j}$ as the set of time intervals between the branch points, defined formally as follows:

$$\mathcal{B}_{t,j} = \left\{ \mathbb{I}_{k_1}^{k_2} \subset \mathbb{I}_t^{t+N} \;\middle|\; \begin{array}{l} \exists j_1, j_2 : (k_1, \{j, j_1\}), (k_2, \{j, j_2\}) \in \mathcal{T}_t, \\ k_2 = \min\left(t+N, \min\limits_{k>k_1, (k,\{j,l\})\in\mathcal{T}_t} k\right) \end{array} \right\}. \tag{11}$$

For example, if the modes are revealed at time step $k = t+1$, we have $\mathcal{T}_t = \{(t, \{1, j\})\ \forall j \in \mathbb{I}_2^J\}$ and $\mathcal{B}_{t,j} = \{\mathbb{I}_t^{t+N}\}\ \forall j \in \mathbb{I}_1^J$. Then for each mode j, we can split the policy matrices as the sums $\mathbf{M}_t^j = \sum_{b=1}^{|\mathcal{B}_{t,j}|} \bar{\mathbf{M}}_t^{j,b}$ and $\mathbf{K}_t^j = \sum_{b=1}^{|\mathcal{B}_{t,j}|} \bar{\mathbf{K}}_t^{j,b}$, where $\bar{\mathbf{M}}_t^{j,b}$ and $\bar{\mathbf{K}}_t^{j,b}$ have the same shape as (24) and (23) but consist only of policy parameters corresponding to the interval $b \in \mathcal{B}_{t,j}$. We denote this policy parameterization as $\boldsymbol{\Theta}_t(x_t, o_t; \mathcal{T}_t)$. The tree structure $\mathcal{T}_t$ is assumed to be inferred from the predictions (5) using some measure of distance between distributions (e.g., Wasserstein distance [47]).

C. Collision Avoidance Formulation

We assume that we are given or can infer the rotation matrices for the ith TV for each mode along the prediction horizon as $\{\{R_{k|t,j}^i\}_{k=1}^N\}_{j=1}^J$. For collision avoidance between the EV and the ith TV, we impose the following chance constraint:

$$\mathbb{P}(g_{k|t}^i(P_{k|t}, o_{k|t}^i) \geq 1\ ) \geq 1-\epsilon \quad \forall k \in \mathbb{I}_1^N \tag{12}$$

where the EV's position $P_{k|t} = [X_{k|t}, Y_{k|t}]$ is obtained from $\mathcal{G}^\gamma(\Delta x_{k|t} + x_{t+k}^{\mathrm{ref}})$, and

$$g_{k|t}^i(P, o) = \left\| \begin{bmatrix} \frac{1}{a_{\mathrm{ca}}} & 0 \\ 0 & \frac{1}{b_{\mathrm{ca}}} \end{bmatrix} R_{k|t,\sigma_t}^i (P - o) \right\|^2 \tag{13}$$

$a_{\mathrm{ca}} = a_{\mathrm{TV}} + d_{\mathrm{EV}}$ and $b_{\mathrm{ca}} = b_{\mathrm{TV}} + d_{\mathrm{EV}}$ are semiaxes of the ellipse containing the TV's extent with a buffer of d_{EV}. $g_{k|t}(P, o) \geq 1$ implies that the EV's extent (modeled as a disk of radius d_{EV} and center P) does not intersect the TV's extent which is modeled as an ellipse with semiaxes a_{TV} and b_{TV} and

center o, oriented by $R_{k|t,\sigma_t}$. The EV is modeled as a circle for robustifying the collision avoidance constraints against the linearization error in EV heading predictions.[1] This constraint is nonconvex because of the integral of the nonlinear function $g^i_{k|t}(\cdot)$ over the multimodal distribution of $(P_{k|t}, o_{k|t}, p_t)$. To address the nonlinearity, we use the convexity of $g^i_{k|t,j}(\cdot)$ to construct its affine underapproximation $l^i_{k+1|t,j}(\cdot)$ by defining $P^i_{k|t,j} = \mu_{k|t,j} + (1/(g^i_{k|t,j}(P^{\text{ref}}_{k|t}, \mu^i_{k|t,j}))^{1/2})(P^{\text{ref}}_{k|t} - \mu^i_{k|t,j})$ to get

$$l^i_{k|t,j}(P,o) = \partial_P g^i_{k|t}\left(P^i_{k|t,j}, \mu^i_{k|t,j}\right)\left(P - P^i_{k|t,j}\right) + \partial_o g^i_{k|t}\left(P^i_{k|t,j}, \mu^i_{k|t,j}\right)\left(o - \mu^i_{k|t,j}\right). \quad (14)$$

Proposition 1: For the affine function $l^i_{k|t,j}(P,o)$ defined in (14), the multimodal chance constraint can be inner approximated $\forall k = t+1,\dots,t+N$ as follows:

$$\sum_{j=1}^{J} p_{t,j}\mathbb{P}\left(l^i_{k|t,j}\left(P_{k|t,j}, o^i_{k|t,j}\right) \geq 0\right) \geq 1-\epsilon$$
$$\Rightarrow \sum_{j=1}^{J} p_{t,j}\mathbb{P}\left(g^i_{k|t,j}\left(P_{k|t,j}, o_{k|t,j}\right) \geq 1\right) \geq 1-\epsilon. \quad (15)$$

Proof: First note that $P^i_{k|t,j}$ is defined such that $g^i_{k|t,j}(P^i_{k|t,j}, \mu^i_{k|t,j}) = 1$. For any convex function $f(x)$, we have $\forall x_0, x : f(x) \geq f(x_0) + \partial_x f(x_0)(x - x_0)$. Since $g^i_{k|t,j}(\cdot)$ is convex, we have $g^i_{k|t,j}(P,o) \geq g^i_{k|t,j}(P^i_{k|t,j}, \mu^i_{k|t,j}) + l^i_{k|t,j}(P,o) = 1 + l^i_{k|t,j}(P,o)$. So $l^i_{k|t,j}(P,o) \geq 0 \Rightarrow g^i_{k|t,j}(P,o) \geq 1$, and $\forall k = t+1,\dots,t+N$

$$\sum_{j=1}^{J} p_{t,j}\mathbb{P}\left(l^i_{k|t,j}\left(P^i_{k|t}, o^i_{k|t,j}\right) \geq 0\right) \geq 1-\epsilon$$
$$\Rightarrow \sum_{j=1}^{J} p_{t,j}\mathbb{P}\left(g^i_{k|t,j}\left(P^i_{k|t}, o^i_{k|t,j}\right) \geq 1\right) \geq 1-\epsilon.$$

We define the curve $\gamma(\cdot)$ using piecewise linear segments so that $\mathcal{G}^\gamma(\Delta x_{k|t} + x^{\text{ref}}_{t+k}) = \mathcal{G}^\gamma(x^{\text{ref}}_{t+k}) + \partial_x \mathcal{G}^\gamma(x^{\text{ref}}_{t+k})\Delta x_{k|t}$, and the constraint (15) is affine in the policy parameters $\boldsymbol{\Theta}_t(x_t, o_t; \mathcal{T}_t)$. Next, we discuss the reformulation of the multimodal affine chance constraints (9), (15).

D. Reformulation of Multimodal Chance Constraints

We propose a novel convex inner approximation for multimodal chance constraints, with the key feature of simultaneous risk allocation for reduced conservatism. The constraints (9), (15) can be generically represented as the multimodal affine chance constraint

$$\sum_{j=1}^{J} p_{t,j}\mathbb{P}\begin{bmatrix} a_0 + a_1^\top \mathbf{h}^j_t + (a_2^\top \mathbf{M}^j_t + a_3^\top)\mathbf{w}_t \\ + (a_4^\top \mathbf{K}^j_t + a_5^\top)\mathbf{L}^j_t \mathbf{n}_t \end{bmatrix} \geq b \geq 1-\epsilon$$
$$\Leftrightarrow \sum_{j=1}^{J} p_{t,j} r_{t,j} \geq 1-\epsilon \quad (16a)$$

$$\mathbb{P}\begin{bmatrix} a_0 + a_1^\top \mathbf{h}^j_t + (a_2^\top \mathbf{M}^j_t + a_3^\top)\mathbf{w}_t \\ + (a_4^\top \mathbf{K}^j_t + a_5^\top)\mathbf{L}^j_t \mathbf{n}_t \end{bmatrix} \geq b \geq r_{t,j}$$
$$\Leftrightarrow a_0 + a_1^\top \mathbf{h}^j_t - b \geq \Phi^{-1}(r_{t,j}) \left\| \begin{bmatrix} \boldsymbol{\Sigma}_t(\mathbf{M}^{j\top}_t a_2 + a_3) \\ \boldsymbol{\Sigma}_{t,j}\mathbf{L}^{j\top}_t(\mathbf{K}^{j\top}_t a_4 + a_5) \end{bmatrix} \right\|_2 \quad (16b)$$

where $\Phi^{-1}(\cdot)$ is the quantile function for $\mathcal{N}(0,1)$, and $r_{t,j}$ are the risk levels $\forall j \in \mathbb{I}^J_1$. We assume that $1-\epsilon \geq (1/2)$ and $r_{t,j} \geq (1/2)$, $\forall j \in \mathbb{I}^J_1$. As such, this constraint is nonconvex in the policy parameters $\boldsymbol{\Theta}_t(x_t, o_t; \mathcal{T}_t)$ and risk levels $r_{t,j}$ because of (16b). The fixed-risk allocation approach [12], [29] fixes the risk level $r_{t,j} = 1-\epsilon$ $\forall j \in \mathbb{I}^J_1$ to obtain a convex inner approximation of the multimodal chance constraint. However as depicted in Fig. 4, this approach can be conservative and compromises the feasibility of the SMPC optimization problem because the risk levels are allocated disregarding the probability of the individual modes. Alternatively, iterative solution strategies [35] have been proposed for variable risk allocation, where alternating subproblems are solved by fixing either the policy parameters or risk levels. This enhances the feasibility of the optimization problem but at the price of significant computational cost. Next, we propose a convex inner approximation to the multimodal chance constraint (16a), (16b) for simultaneous risk allocation and policy synthesis, to alleviate the computational cost of iterative approaches, but also improve the feasibility of constraint compared to the fixed allocation approach.

First, we focus on reformulating (16b). We recall that the policy parameters can be split as $\mathbf{M}^j_t = \sum_{b=1}^{|\mathcal{B}_{t,j}|} \bar{\mathbf{M}}^{j,b}_t$ and $\mathbf{K}^j_t = \sum_{b=1}^{|\mathcal{B}_{t,j}|} \bar{\mathbf{K}}^{j,b}_t$, and begin by introducing new variables

$$\eta_{t,j} = \Phi^{-1}(r_{t,j})$$
$$\tilde{\mathbf{M}}^j_t = \Phi^{-1}(r_{t,j})\bar{\mathbf{M}}^{j,|\mathcal{B}_{t,j}|}_t, \quad \tilde{\mathbf{K}}^j_t = \Phi^{-1}(r_{t,j})\bar{\mathbf{K}}^{j,|\mathcal{B}_{t,j}|}_t$$

to rewrite the constraint (16b) as follows:

$$a_0 + a_1^\top \mathbf{h}^j_t - b \geq \left\| \begin{bmatrix} \boldsymbol{\Sigma}_t(\tilde{\mathbf{M}}^{j\top}_t a_2 + \eta_{t,j} \sum_{b=1}^{|\mathcal{B}_{t,j}|-1} \bar{\mathbf{M}}^{j,b\top}_t a_2 + a_3\eta_{t,j}) \\ \boldsymbol{\Sigma}_{t,j}\mathbf{L}^{j\top}_t(\tilde{\mathbf{K}}^{j\top}_t a_4 + \eta_{t,j} \sum_{b=1}^{|\mathcal{B}_{t,j}|-1} \bar{\mathbf{K}}^{j,b\top}_t a_4 + a_5\eta_{t,j}) \end{bmatrix} \right\|_2. \quad (17)$$

The variable $\eta_{t,j}$ can be interpreted as the number of standard deviations by which the affine constraint is tightened. Since $r_{t,j} \geq (1/2)$, we have $\eta_{t,j} \geq 0$, and additionally, let $\eta_{t,j} \leq \eta_{\max}$ to ignore the tail of the Gaussian distribution. The inequality (17) is nonconvex in the new variables because of the bilinear terms $\eta_{t,j}\bar{\mathbf{M}}^{j,b\top}_t$ and $\eta_{t,j}\bar{\mathbf{K}}^{j,b\top}_t$. However, fixing either variable in these terms yields a convex, second-order cone (SOC) constraint. We use this insight to obtain a convex inner approximation of this nonconvex inequality as follows.

Proposition 2: A convex inner approximation of (17) can be obtained as the intersection of the two SOC constraints in

[1]For using general convex sets, the dual approach for collision avoidance [27] can be used that expresses the intersection between uncertain convex-shaped agents as the problem of finding a hyperplane that *robustly* separates the two uncertain convex sets.

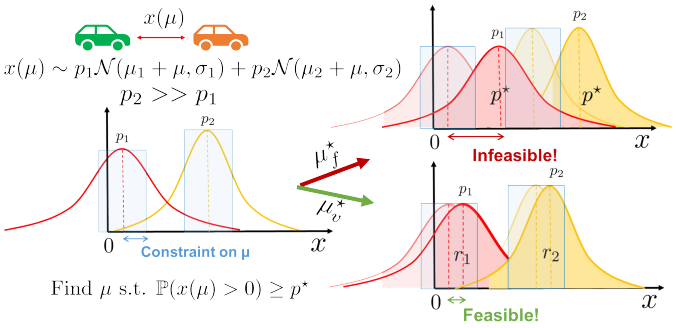

Fig. 4. For $x(\mu)$ given by a GMM on the left (e.g., predicted distance from the lead vehicle), the figure depicts the fixed-risk (top-right) and variable-risk (bottom-right) formulations for shaping $x(\mu)$ for satisfying the constraint $\mathbb{P}(x(\mu) > 0) \geq p^\star$ by optimizing μ within the blue feasible region (e.g., dictated by actuation constraints). The variable-risk formulation can choose a smaller $\mu = \mu_v^\star$ within constraints by exploiting the difference in mode probabilities, since $p_2 \gg p_1$, assigning a larger risk level r_2 (shaded yellow region) to mode 2 yields feasible distributions. The fixed-risk formulation assigns $r_1 = r_2 = p^\star$ but the resulting $\mu = \mu_f^\star$ violates the constraints.

the variables $\{\mathbf{h}_t^j, \tilde{\mathbf{M}}_t^j, \tilde{\mathbf{K}}_t^j, \{\bar{\mathbf{M}}_t^{j,b}, \bar{\mathbf{K}}_t^{j,b}\}_{b=1}^{|\mathcal{B}_{t,j}|-1}, \eta_{t,j}\}$

$$
\begin{aligned}
&a_0 + a_1^\top \mathbf{h}_t^j - b \\
&\geq \left\| \begin{bmatrix} \mathbf{\Sigma}_t(\tilde{\mathbf{M}}_t^{j\top} a_2 + a_3\eta_{t,j}) \\ \mathbf{\Sigma}_{t,j}\mathbf{L}_t^{j\top}(\tilde{\mathbf{K}}_t^{j\top} a_4 + a_5\eta_{t,j}) \end{bmatrix} \right\|_2 \\
&a_0 + a_1^\top \mathbf{h}_t^j - b \\
&\geq \left\| \begin{bmatrix} \mathbf{\Sigma}_t(\tilde{\mathbf{M}}_t^{j\top} a_2 + \eta_{\max} \sum_{b=1}^{|\mathcal{B}_{t,j}|-1} \bar{\mathbf{M}}_t^{j,b\top} a_2 + a_3\eta_{t,j}) \\ \mathbf{\Sigma}_{t,j}\mathbf{L}_t^{j\top}(\tilde{\mathbf{K}}_t^{j\top} a_4 + \eta_{\max} \sum_{b=1}^{|\mathcal{B}_{t,j}|-1} \bar{\mathbf{K}}_t^{j,b\top} a_4 + a_5\eta_{t,j}) \end{bmatrix} \right\|_2 .
\end{aligned} \tag{18}
$$

Proof: First, we note the following auxilliary result. For a convex function $f(\cdot)$ and $x \in [x_{\min}, x_{\max}] \subset \mathbb{R}$, if $f(x_{\min} y) \leq 0$, $f(x_{\max} y) \leq 0$, then $f(xy) \leq 0$ for any $x \in [x_{\min}, x_{\max}]$. Now suppose that (18) holds, and use the above result for an arbitrary $\tilde{\eta}_{t,j} = \gamma\eta_{\max} + (1-\gamma)0$ with $\gamma \in [0,1]$ to get

$$
\begin{aligned}
&a_0 + a_1^\top \mathbf{h}_t^j - b \\
&\geq \left\| \begin{bmatrix} \mathbf{\Sigma}_t \left(\tilde{\mathbf{M}}_t^{j\top} a_2 + \tilde{\eta}_{t,j} \sum_{b=1}^{|\mathcal{B}_{t,j}|-1} \bar{\mathbf{M}}_t^{j,b\top} a_2 + a_3\eta_{t,j} \right) \\ \mathbf{\Sigma}_{t,j}\mathbf{L}_t^{j\top} \left(\tilde{\mathbf{K}}_t^{j\top} a_4 + \tilde{\eta}_{t,j} \sum_{b=1}^{|\mathcal{B}_{t,j}|-1} \bar{\mathbf{K}}_t^{j,b\top} a_4 + a_5\eta_{t,j} \right) \end{bmatrix} \right\|_2 .
\end{aligned}
$$

Since $\tilde{\eta}_{t,j}$ is arbitrary, the desired result is obtained by setting $\tilde{\eta}_{t,j} = \eta_{t,j}$.

With the new variable definitions, constraint (16a) takes the form $\sum_{j=1}^J p_{t,j}\Phi(\eta_{t,j}) \geq 1-\epsilon$, which is convex in $\eta_{t,j}$, but difficult to enforce since $\Phi(\cdot)$ lacks a closed-form expression. For $\eta \in [0, \eta_{\max}]$, we approximate $\Phi(\eta)$ by a concave function $\Psi(\eta) = \min_{i=1,\ldots,v}\{q_i^1\eta + q_i^0\}$ such that $\Phi(\eta) \geq \Psi(\eta)$, and

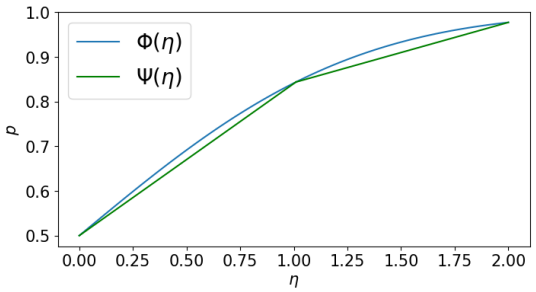

Fig. 5. $\Psi(\eta)$ as a concave underapproximation of $\Phi(\eta)$.

replace (16a) with the convex inner approximation

$$
\sum_{j=1}^J p_{t,j}\Psi(\eta_{t,j}) \geq 1-\epsilon. \tag{19}
$$

A candidate approximation of $\Phi(\cdot)$ over $[0,2]$ with $v = 2$ affine functions is shown in Fig. 5. Thus, the nonconvex constraints (16a), (16b) can be replaced by the convex inner approximations provided by the SOC constraints (19), (18).

E. SMPC Optimization Problem

The cost (6a) of the SMPC optimization problem (6) can be chosen to penalize deviations of the EV state and input trajectories from the reference trajectory (4) as follows:

$$
C_t(\mathbf{x}_t, \mathbf{u}_t) = \sum_{k=0}^{N-1} \Delta x_{k+1|t}^\top Q \Delta x_{k+1|t} + \Delta u_{k|t}^\top R \Delta u_{k|t}
$$

where $Q, R \succ 0$. Let $\mathbf{\Theta}_t^{\text{MPC}}(x_t, o_t; \mathcal{T}_t)$ denote the set of policy parameters and risk levels

$$
\boldsymbol{\theta}_t := \left\{ \mathbf{h}_t^j, \tilde{\mathbf{M}}_t^j, \tilde{\mathbf{K}}_t^j, \left\{ \bar{\mathbf{M}}_t^{j,b}, \bar{\mathbf{K}}_t^{j,b} \right\}_{b=1}^{|\mathcal{B}_{t,j}|-1}, \eta_{t,j} \right\}_{j=1}^J
$$

such that they satisfy the following: 1) the reformulations (18), (19) of the multimodal state-input and collision avoidance constraints (9), (15) and 2) structural constraints given by $\mathcal{T}_t$. We use the single-shooting/batch formulation for the optimal control problem using the linearized dynamics (8) so that the only decision variables in the optimization problem are the policy parameters $\boldsymbol{\theta}_t$. Thus, the SMPC (7) for the EV can be synthesized by solving the SOCP

$$
\begin{aligned}
&\min_{\boldsymbol{\theta}_t} \sum_{j=1}^J p_{t,j}\mathbb{E}\left[C_t(\mathbf{x}_{t,j}, \mathbf{u}_{t,j})\right] \\
&\text{s.t } \boldsymbol{\theta}_t \in \mathbf{\Theta}_t^{\text{MPC}}(x_t, o_t; \mathcal{T}_t).
\end{aligned} \tag{20}
$$

IV. Numerical Validation

In this section, we investigate the proposed algorithm, both qualitatively and quantitatively. To assess the benefits of our proposed SMPC formulation, we demonstrate our approach in three different scenarios: 1) longitudinal control with a TL and a following vehicle; 2) unprotected left turn at an intersection; and 3) LC on a straight road. In scenario 1), we validate the proposed algorithm in a simple 1-D simulation and show the

qualitative behavior of our SMPC in managing the multimodal predictions. In scenarios 2) and 3), we use CARLA [48] for the simulator and adopt the motion predictor MultiPath [8] to predict the multimodal future motions of surrounding vehicles. In these scenarios, we provide a quantitative study of our approach against baselines.

A. Qualitative Analysis: Longitudinal Control With a TL and a Following Vehicle

1) Setup: Consider the situation in Fig. 1(a), where the EV is approaching a TL with a tailgating TV behind. All vehicles and the TL are simulated in a simple 1-D simulator. Both vehicles are modeled as double integrators with Euler discretization (@$dt = 0.1$ s) as follows:

$$\begin{aligned} x_t &= \begin{bmatrix} s_t & v_t \end{bmatrix}^\top, \quad u_t = a_t \\ x_{t+1} &= \begin{bmatrix} 1 & dt \\ 0 & 1 \end{bmatrix} x_t + \begin{bmatrix} 0.5\ dt^2 \\ dt \end{bmatrix} u_t \\ o_t &= \begin{bmatrix} s_t^o & v_t^o \end{bmatrix}^\top, \quad u_t^o = a_t^o \\ o_{t+1} &= \begin{bmatrix} 1 & dt \\ 0 & 1 \end{bmatrix} o_t + \begin{bmatrix} 0.5\ dt^2 \\ dt \end{bmatrix} u_t^o + w_t^o \\ w_t^o &\sim \mathcal{N}(0, 0.6\ I_2) \end{aligned} \tag{21}$$

where each state comprises the longitudinal position and speed, each input is the acceleration, and w_t^o is an additive process noise in the TV dynamics. For our simulation, the initial states of the EV and the TV are set to $x_0 = [0,\ 13.9]$ and $o_0 = [-12.75, 14]$ so that 1) TV has a 0.7 s time headway behind the EV and 2) there is enough distance for the EV to brake at 0.7 g and stop at the TL, which is located 50 m ahead of the EV, i.e., $s_f = 50$ m.

The EV is subject to state-input constraints $\mathcal{X} \times \mathcal{U} = \{(x, u) : v \in [v_{\min}, v_{\max}], a \in [a_{\min}, a_{\max}]\}$ and collision avoidance constraints $\mathcal{C} = \{(x, o) : s - o \geq d_{\text{safe}}\}$, where $v_{\min} = 0$ m/s, $v_{\max} = 14$ m/s, $a_{\min} = -8$ m/s^2, $a_{\max} = 4$ m/s^2, and $d_{\text{safe}} = 7$ m.

For simplicity, we assume that the driver in the TV has good decision-making skills based on the previous observations. In particular, we assume the following.

1) When the TV's driver is confident that the TL will remain yellow until the TV crosses with a probability of 1, the TV will maintain its speed.
2) When the TV's driver is not confident that the TL will remain yellow, they will choose to brake. Here, we assume that the probability of either red or yellow light is 0.5 conditioned on the TV choosing to brake.
3) The TV's driver will make a decision when the TV passes a certain point, i.e., $s_t^o \geq s_{\text{dec}}$.

Under this assumption, there are three possible modes.

1) *Mode 0:* TV keeps speed, TL stays yellow.
2) *Mode 1:* TV brakes, TL stays yellow.
3) *Mode 2:* TV brakes, TL goes red before EV crosses.

The EV does not know the true mode $\sigma \in \{0, 1, 2\}$. The EV estimates the probabilities of each mode as $p_t = [p_{t,0}, p_{t,1}, p_{t,2}]$ using Bayes' rule via observations of the TV's state history $o_0, o_1, ..o_t$ after crossing s_{dec}. The tree structure $\mathcal{T}_t$ for the predictions is determined by rolling out the TV's acceleration commands and branching into the three modes based on when it crosses s_{dec}.

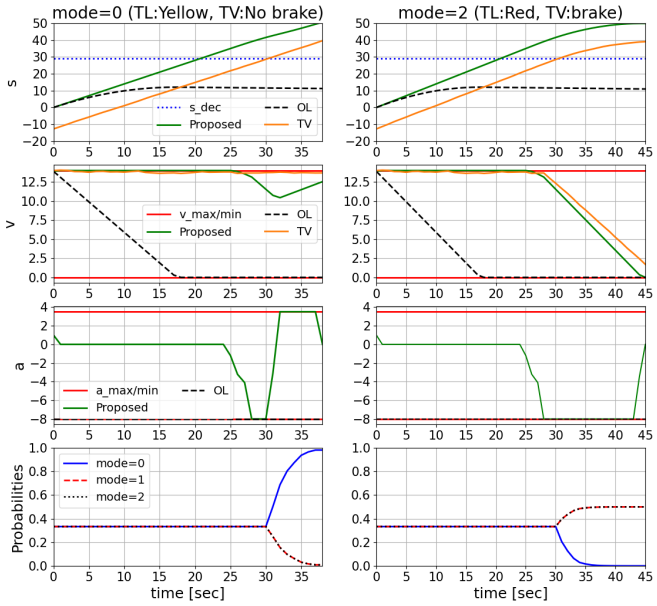

Fig. 6. Closed-loop plots for the longitudinal control example for modes $\sigma = 0, 2$ by solving (20) for the SMPC. *Proposed* is our proposed approach and *OL* is the open-loop approach. The TL is located at $s_f = 50$ m. The EV is unaware of the true mode σ, but estimates the mode probabilities from TV observations. Using the proposed approach, the EV is able to cross the TL for $\sigma = 0$ and safely stop before the TL for $\sigma = 2$. Code: https://github.com/shn66/AV_SMPC_Demos/tree/TL_eg.

The chance constraints are imposed with risk level $\epsilon = 0.01$. For deriving the variable-risk reformulations of multimodal chance constraints (9), (15) as shown in Section III-D, we use $\Psi(\eta)$ as depicted in Fig. 5 as the concave underapproximation of the cdf $\Phi(\eta)$ over $\eta \in [0, 2]$. For stopping at s_f in mode 2, we enforce the terminal constraint $\mathcal{X}_f = \{x = [s, v] \in \mathcal{X} : v^2 \leq -2a_{\min}(s_f - s)\}$.

The SMPC cost is given as $C_t(\mathbf{x}_{t,j}, \mathbf{u}_{t,j}) = \sum_{k=t}^{t+N} -Qs_{k+1|t,j} + Ru_{k|t,j}^2$ over prediction horizon $N = 12$ with $Q = 10$ and $R = 20$ to penalize slow progress and control effort.

2) Simulations: We run two different simulation scenarios, where true modes are $\sigma = 0$ and $\sigma = 2$, respectively. Note that the EV does not know the true mode and estimates the mode after TV crosses the decision point $s_t^o \geq s_{\text{dec}}$. We compare the proposed SMPC in (20) (*Proposed* in Fig. 6) with an OL approach (*OL* in Fig. 6), where the EV solves an SMPC with fixed-risk levels for each mode, and optimizes over a single OL sequence $\mathbf{h}_t$, i.e., the gains $K_{k|t}^j$ and $M_{l,k|t}^j$ in (10) are eliminated. The results are illustrated in Fig. 6.

3) Discussion: As depicted in Fig. 6, the OL approach is unable to exploit the mode probabilities and is infeasible throughout the simulation, leading to a collision with the TV. In contrast, the proposed approach accordingly accelerates to cross the yellow TL in the first realization, while it decelerates to a stop in the second realization (without knowing the true mode σ) after the TV crosses the decision point $s_t^o \geq s_{\text{dec}}$ (around $t = 30$ s). This closed-loop behavior results from the

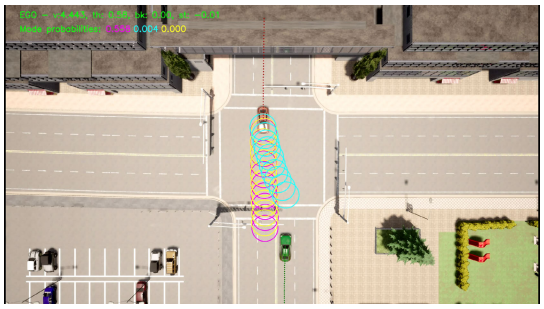

(a)

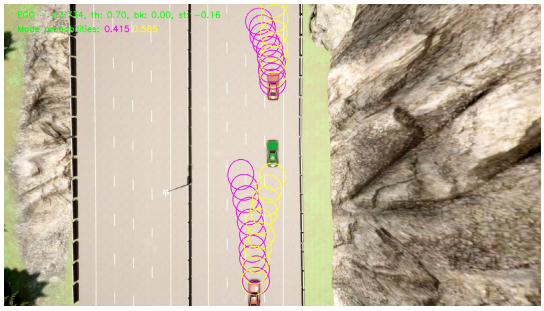

(b)

Fig. 7. Carla simulation setup for unprotected left turn and LC for EV (green) in the presence of TVs (orange) and multimodal predictions (depicted by the ellipses). Code: https://github.com/shn66/SMPC_MMPreds. (a) Unprotected left. (b) LC.

estimation of the mode probabilities and the incorporation of the multimodal probability estimates in the chance constraints as in (19).

B. Quantitative Analysis: Unprotected Left Turn and LC With Surrounding Vehicles

1) Setup: Consider the two scenarios as depicted in Fig. 7.

1) *Unprotected Left*: The EV makes a left turn through the intersection while avoiding an oncoming TV.
2) *LC*: The EV changes into the left lane in the presence of two TVs: one ahead in the same lane and another behind in the adjacent lane.

All vehicles are simulated in a synchronous fashion in CARLA, ensuring that all processing (prediction, planning, and control) is complete before advancing the simulation. Thus, our results only consider the impact of the control and not the time delays incurred in computation.

The TVs' controls are given by a simple nonlinear MPC to go straight, with a kinematic bicycle model for predictions and simple distance-based collision avoidance constraints. From the EV's perspective, the predictions of the TV's motion are given by a GMM for multimodal trajectory predictions of the form (5). We obtain this multimodal distribution along with mode probabilities online using the MultiPath prediction model from [8]. Given the predicted multimodal distributions for the TVs, we use the framework introduced in Section III to generate feedback control policies with fixed $\mathcal{T}_t = \{(t+3, \{1, j\})\ \forall j \in \mathbb{I}_2^J\}$, and use Fig. 5 for the cdf approximation. A dynamically feasible EV reference trajectory (4) is obtained by solving a nonlinear trajectory optimization problem for a kinematic bicycle using IPOPT [49] to track a high-level route (provided by the CARLA waypoint API). Given the EV reference (4) and TV predictions (5), the SMPC optimization problem (20) is solved using Gurobi [50] to compute the acceleration and steering controls.

2) Policies: We evaluate and compare the following set of policies for this unprotected left scenario.

1) *Proposed:* Our proposed framework, given by solving (20) which optimizes over both, policies and risk levels, for the multimodal chance constraint (16a), (16b).
2) *Fixed Risk:* An ablation of our approach, which optimizes over policies but with fixed risk levels $r_{t,j} = 1-\epsilon$ for the multimodal chance constraint (16a), (16b).
3) *OL:* An ablation of our approach, where the gains $K^j_{k|t}$, $M^j_{l,k|t}$ are eliminated and risk levels are fixed too.

Note that **Proposed** and **OL** in this section are the same algorithms that were compared in Section IV-A.

3) Evaluation Metrics: We introduce a set of closed-loop behavior metrics to evaluate the policies. A desirable planning framework enables high mobility without being overconservative, allowing the timely completion of the driving task while maintaining passenger comfort. The computation time should also not be exorbitant to allow for real-time processing of updated scene information. The following metrics are used to assess these factors.

1) *Mobility:* 1) $\tilde{\mathcal{T}}_{\text{episode}}$: Time the EV takes to reach its goal normalized by the time taken by the reference and 2) $\Delta\tau$: Deviation (in Hausdorff distance) of the closed-loop trajectory from the reference trajectory. A large deviation $\Delta\tau$ indicates a longer trajectory, leading to an extended time required to complete the maneuver.
2) *Comfort:* 1) $\tilde{\mathcal{A}}_{\text{lat}}$: Peak lateral acceleration normalized by the peak lateral acceleration in reference; 2) $\bar{\mathcal{J}}_{\text{long}}$: Average longitudinal jerk; and 3) $\bar{\mathcal{J}}_{\text{lat}}$: Average lateral jerk. High values are undesirable, linked to sudden braking or steering.
3) *Safety:* 1) $\mathcal{F}$: Feasibility % of the SMPC optimization problem. A high $\mathcal{F}$ value is desirable, as infeasibility of the SMPC can potentially lead to accidents; 2) $\bar{d}_{\text{min}}$: Closest distance between the EV and TV of each algorithm, provided that the algorithm remains feasible. A higher $\bar{d}_{\text{min}}$ indicates that the algorithm should be more conservative to maintain safety. This caution can lead to reduced feasibility when the algorithm encounters congested urban road driving scenarios; and 3) $\mathcal{P}$: Average collision probability (6d) (in %) of the MPC solution; $\mathcal{P}/100 \approx \epsilon$ indicates tighter chance constraints satisfaction.
4) *Solver Performance:* 1) $\bar{\mathcal{T}}_{\text{solve}}$: Average time taken by the solver; lower is better.

4) Discussion: Now, we present the results of the various SMPC policies. For each scenario, we roll out each policy for 50 different initial conditions by varying the following: 1) starting positions within $[-5, 5]$ m and 2) nominal speed in $[8, 10]$ m/s]. For fairness and consistency of the metrics, this range of initial conditions was chosen so that none of the policies led to collisions in both scenarios. For all the policies, we use a prediction horizon of $N = 10$, a discretization time

TABLE I
CLOSED-LOOP PERFORMANCE COMPARISON ACROSS ALL SCENARIOS

Scenario	Policy	Mobility		Comfort			Safety			Solver Performance
		$\tilde{\mathcal{T}}_{episode}$	$\Delta\tau$ (m)	$\tilde{\mathcal{A}}_{lat}$	$\bar{\mathcal{J}}_{long}$ ($\frac{m}{s^3}$)	$\bar{\mathcal{J}}_{lat}$ ($\frac{m}{s^3}$)	$\mathcal{F}$ (%)	$\bar{d}_{min}$ (m)	$\mathcal{P}$(%)	$\bar{\mathcal{T}}_{solve}$ (ms)
Unprotected left	**OL**	1.53	1.96	1.31	8.09	**6.62**	81.14	3.88	0.1	**13.6**
	Fixed risk	1.10	3.09	1.41	4.23	9.04	98.37	3.09	0.44	31.5
	Proposed	**1.09**	**3.07**	**1.21**	**3.67**	8.58	**99.88**	3.07	1.63	39.9
Lane change	**OL**	1.32	7.71	8.16	4.41	6.45	82.55	3.42	0.88	**35.6**
	Fixed risk	1.07	3.03	5.71	3.80	4.93	96.08	3.21	1.31	325.20
	Proposed	**1.06**	**2.92**	**4.17**	**3.25**	**3.27**	**98.76**	3.19	1.84	397.19

step of $dt = 0.2$ s, and a risk level of $\epsilon = 0.02$ for the chance constraints in the SMPC.

The performance metrics, averaged across the initial conditions, are shown in Table I. In terms of mobility, **Proposed** is able to improve or maintain mobility compared to the ablations. There is a noticeable improvement in comfort and safety metrics, as the **Proposed** can stay close to the TV-free reference trajectory without incurring high acceleration/jerk and keeping a safe distance from the TV. **Proposed** was also able to find feasible solutions for the SMPC optimization problem more often in our experiments because the formulation optimizes over policies and risk levels for the multimodal constraints. Additionally, we see that the average collision probabilities of the computed solutions are closer to the chosen risk level $\epsilon = 0.02$ (or 2%) in (6d). Finally, we see that the **OL** is the fastest in solve time (because of the missing policy and risk variables). However, we see that introducing the additional risk-level variables only marginally increases the solve time on comparing **Proposed** and **Fixed risk**. The higher solve times for the proposed approach in the LC scenario are because of the additional TV and its associated multimodal predictions. To remedy this issue for the hardware experiments in Section V, we use a multithreaded implementation as described in Section V to solve the SMPC.

The results highlight the benefits of optimizing over policies and incorporating the variable risk formulation in the SMPC formulation (6) for the EV, toward collision avoidance with multimodal predictions of the TV. The executed maneuvers for each policy in both scenarios can be seen at https://shorturl.at/pJQVW.

V. EXPERIMENTAL VALIDATION

In this section, we validate our approach in hardware vehicle experiments to assess the benefits of our proposed SMPC formulation. The experiment videos can be accessed at https://shorturl.at/ctQ57.

A. Test Scenario and Key Takeaways

In the hardware experiment, we consider the same lane-change scenario introduced in Section IV-B, wherein EV initiates a LC maneuver with a leading TV ahead of the EV in the same lane and a trailing TV behind the EV in the adjacent lane as illustrated in Fig. 8. In this scenario, EV predicts multimodal behaviors of other TVs and tries to minimize the risk of collisions for every possible mode. As illustrated in Fig. 8, EV predicts two different modes of TVs: keeping their lanes or changing lanes. However, TVs will not change their lane until the end of this scenario.

Fig. 8. Drone view of the testing scenario including EV (red) and 2 TVs (blue) with predictions (yellow and green circles).

We compare the proposed SMPC (**Proposed**) with the **OL**, introduced in Section IV-B. The results in Fig. 9 show that while the **OL** cannot find a feasible solution due to its conservativeness of the constraint tightening formulation, **Proposed** successfully accomplishes the given scenario without any collisions. When **OL** problem becomes infeasible, we change the control policy **OL** to a backup control policy: keeping the current lane and decelerating mildly. This abrupt policy change can deteriorate the comfort indices and it is more likely that tracking previous optimal trajectories from **OL** leads to smoother behaviors. However, due to safety concerns, we tried to stop the vehicle within the current lane.

Furthermore, we study how the predicted mode probability of the leading TV affects the closed-loop behavior. Compared to the case that the leading TV is likely to keep its lane ($p_{\text{lk}} = 0.9$), **Proposed** sets more margin in a lateral direction to avoid the collision in case the leading TV changes lanes ($p_{\text{lk}} = 0.1$) as illustrated in Fig. 10.

B. Hardware Architecture for Experiments

The test vehicle and the hardware setup are illustrated in Fig. 11. The computing unit of the system consists of three computers: a Linux-based laptop, a Linux-based rugged computer, and the dSPACE MicroAutoBox II (MABXII). The laptop is for simulating virtual environments and transmitting all information such as states of surrounding vehicles. The rugged PC is for implementing a planning and control software stack that plans the EV's behavior, generates dynamically feasible, safe trajectories, and calculates acceleration and yaw rate to track the generated trajectories. The MABXII is for implementing an actuator-level controller that calculates

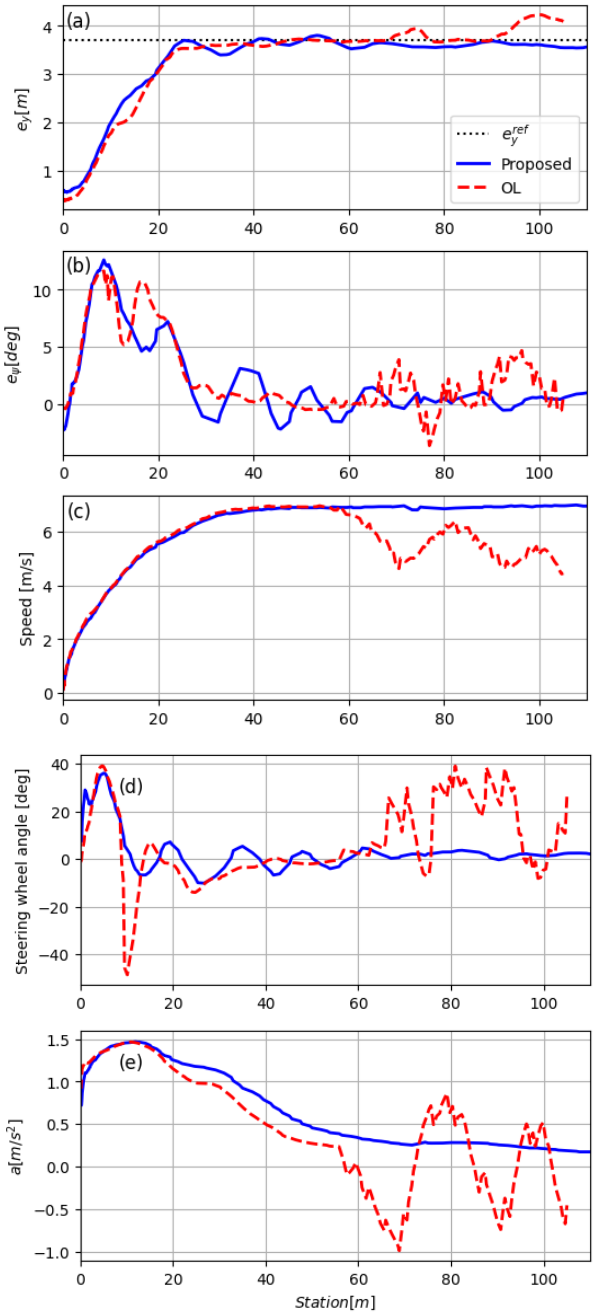

Fig. 9. Comparison: **Proposed** versus **OL**. (a) Lateral error with respect to the centerline of the original lane. e_y^{ref} denotes the reference, (b) heading error with respect to the centerline, (c) vehicle longitudinal speed, (d) steering wheel angle, and (e) longitudinal acceleration. **Proposed** makes the EV keep the lateral distance (e_y) close to the reference while satisfying the multimodal collision avoidance constraints. In contrast, the **OL** becomes infeasible during the task.

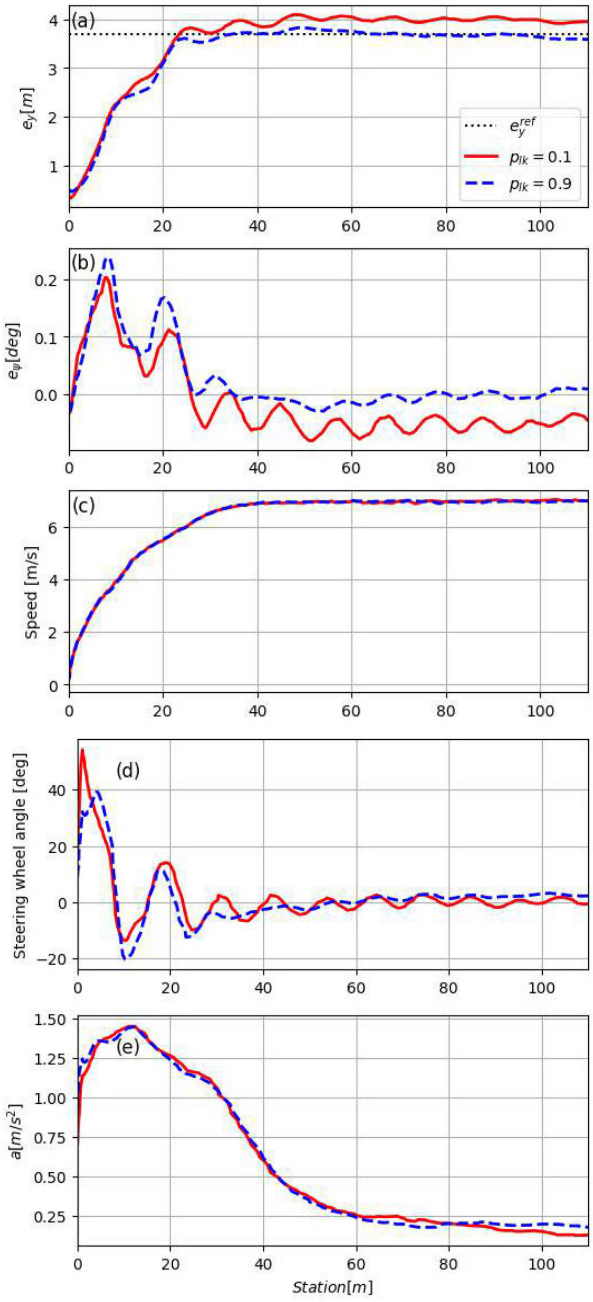

Fig. 10. Comparison: $p_{\text{lk}} = 0.1$ versus $p_{\text{lk}} = 0.9$. (a) Lateral error with respect to the centerline of the original lane. e_y^{ref} denotes the reference, (b) heading error with respect to the centerline, (c) vehicle longitudinal speed, (d) steering wheel angle, and (e) longitudinal acceleration. Compared to the case that the leading TV is likely to keep its lane ($p_{\text{lk}} = 0.9$), **Proposed** sets more margin in a lateral direction to avoid the collision in case the leading TV changes lanes ($p_{\text{lk}} = 0.1$).

actuator control inputs and a fail-safe logic that provides safety features.

The sensors of the system are an OxTS RT3000: a differential GPS to localize the EV and production vehicle sensors to acquire vehicle state information.

C. Software Architecture for Experiments

The overall block diagram of the control architecture and the entire system is illustrated in Fig. 12. In the following sections, we describe the comprehensive details of this experimental setup.

1) Planning and Control Software Stack: The developed hierarchical control system consists of a lane selector, a trajectory planner, and a vehicle controller. First, the lane selector determines the target lane for the EV. Second, given the target lane, the trajectory planner [41] generates a smooth, comfortable trajectory to the target lane by solving a nonlinear optimization problem. The calculated trajectory serves as the reference (4) for the proposed SMPC. Then the proposed

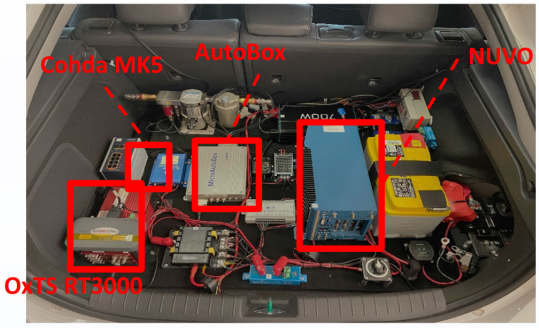

Fig. 11. Hardware setup in the actual vehicle.

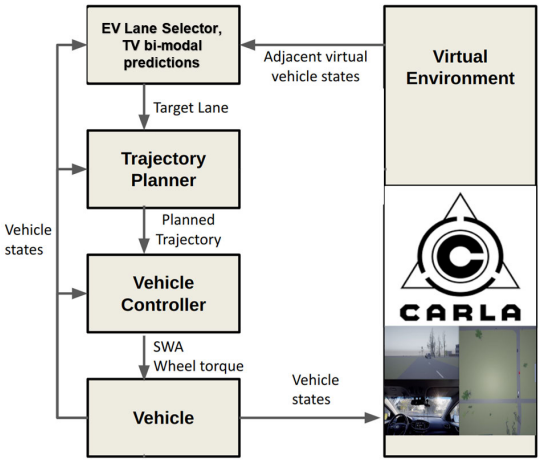

Fig. 12. Diagram of control architecture.

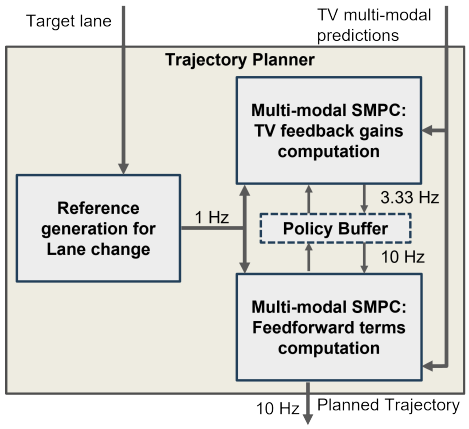

Fig. 13. Trajectory planner architecture.

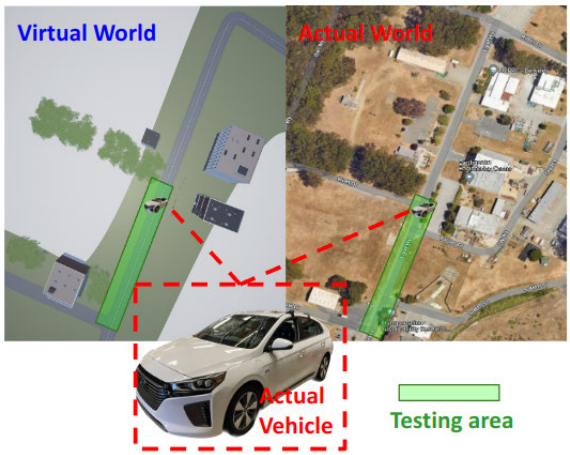

Fig. 14. CARLA image, the satellite image of the testing site (RFS), and the actual vehicle image.

SMPC (20) is solved to determine acceleration and yaw rate commands that satisfy state/input constraints. A kinematic bicycle model (1) is employed for the EV predictions in the SMPC optimization problem, which is modeled with CasADi and solved using Gurobi. For computing the SMPC commands at 10 Hz, we employ a multithreaded architecture that computes the feedforward terms $h^j_{k|t}$ with a fixed-time budget of 100 ms (10 Hz) and the feedback gains $K^j_{k|t}$ and $M^j_{l,k|t}$ with a fixed-time budget of 300 ms (3.33 Hz) as depicted in Fig. 13. Finally, the vehicle actuator controller calculates steering wheel angle and wheel torque commands from the optimal inputs of the proposed SMPC (20).

2) Virtual Environment Simulator (Digital Twin): To conduct real-world vehicle tests safely and efficiently, we employ a VIL system as outlined in [41], which integrates the operation of an actual vehicle with a virtual environment simulation.

The CARLA [48] software is the primary simulator to build virtual environments and simulate a variety of scenarios with ease. The virtual environment simulator constructs all components such as road networks, other vehicles, traffic infrastructures, and buildings to replicate the real-world map. Fig. 14 shows the generated CARLA map, the satellite image of the testing site, and the actual test vehicle.

On the customized map, the CARLA simulates a traffic scenario with the same initial conditions such as the number of spawned vehicles and the locations of the vehicles. It is worth noting that the CARLA simulator exhibits inherent randomness in the motion of each virtual vehicle, resulting in variations in the resulting traffic scenario. We also synchronize the real world with the virtual world in terms of the physical EV. Based on the obtained coordinate data from dGPS/IMU sensors, the simulator generates an agent in the virtual world and teleports the vehicle by updating the position and orientation of the agent every time it receives data from the actual sensors.

D. Experiment Results

Our experiment setup parameters are described as follows. The EV initiates motion with an initial speed of zero. The leading TV begins its movement 10 m ahead of the EV in the same lane, while the trailing TV starts from a position 25 m behind the EV in the adjacent lane. Both TVs maintain a consistent average speed of 4 m/s. Each of the TVs operates in two distinct modes: lane keeping (LK) and LC. The trailing TV equally splits its mode probability, with a 50% chance of LK and a 50% chance of LC. To investigate the impact of varying mode probabilities, we change the probability of the mode chosen by the leading TV.

The conducted tests are executed at the Richmond field station (RFS), as illustrated in Fig. 14. The hardware experiments are primarily divided into two segments. The first segment

involves a comparison between our approach (which optimizes over multimodal policies and risk levels) against a baseline that only optimizes over multimodal OL sequences with fixed risk levels for each mode (i.e., **OL** from Section IV-B). The second segment focuses on assessing the behavioral outcomes resulting from alterations in the probability of the surrounding vehicle's LC mode and LK mode.

*1) **Proposed** Versus **OL**:* Within the identical scenario, we conduct testing using two distinct control policies: **Proposed** in Section IV-B and **OL** in Section IV-B. When the SMPC problem becomes infeasible, a lane-keeping controller with mild braking takes over the control. In an ideal practical application, a human driver should take over the control but due to our hardware limitations, we utilize the lane-keeping controller as a backup controller.

Fig. 9 presents the closed-loop behaviors: a lateral error e_y and a heading error e_ψ with respect to a centerline, vehicle speed, steering wheel angle, and longitudinal acceleration. The graphs clearly illustrate that the **OL** yields infeasible solutions, leading to abrupt and undesirable motions with constraint violations. Conversely, the **Proposed** consistently generates feasible solutions, facilitating smooth motions in accordance with the predefined constraints.

2) Change of Mode Probability: In the section, we proceed with testing under the **Proposed** while varying the lane-keeping probability of the leading TV. Specifically, we compare the case that the leading TV is likely to keep its lane ($p_{\text{lk}} = 0.9$) with the case that the leading TV changes lanes ($p_{\text{lk}} = 0.1$). In Fig. 10's lateral error (e_y) graph, it is evident that the lateral distance is greater in the scenario with a lower lane-keeping probability. This observation aligns with the intuitive analysis that the resulting control policy prioritizes the LC maneuver of the leading vehicle to the lane currently occupied by the EV. Due to the presence of collision avoidance constraints, the EV endeavors to evade the anticipated trajectory of the leading TV by maintaining larger lateral safety margins.

VI. Conclusion

We proposed an SMPC formulation for autonomous driving with multimodal predictions of surrounding vehicles. We provide a convex formulation for simultaneously: 1) optimizing over parameterized feedback policies and 2) allocating risk levels to each mode for multimodal chance constraint satisfaction. This enhances the feasibility and closed-loop performance of the SMPC algorithm, as demonstrated by our simulations and hardware experiments.

Appendix
Matrix Definitions

$$\Delta \mathbf{u}_{t,j} = \mathbf{h}_t^j + \mathbf{M}_t^j \mathbf{w}_t + \mathbf{K}_t^j (\mathbf{o}_{t,j} - \boldsymbol{\mu}_{t,j}) \quad \{\textit{Stacked Control Policy}\}$$

$$\mathbf{h}_t^j = \left[h_{t|t}^{j\top}, \ldots, h_{t+N-1|t}^{j\top} \right]^\top \tag{22}$$

$$\mathbf{K}_t^j = \text{blkdiag}\left(K_{t|t}^j, \ldots, K_{t+N-1|t}^j \right) \tag{23}$$

$$\mathbf{M}_t^j = \begin{bmatrix} O & \cdots & \cdots & \cdots & O \\ M_{t,t+1|t}^j & O & \cdots & \cdots & O \\ \vdots & \vdots & \vdots & \vdots & \\ M_{t,k|t}^j & \cdots M_{k-1,k|t}^j & O & \cdots & O \\ \vdots & \vdots & \vdots & \vdots & \\ M_{t,t+N-1|t}^j & \cdots & \cdots M_{t+N-2,t+N-1|t}^j & & O \end{bmatrix} \tag{24}$$

$$\Delta \mathbf{x}_{t,j} = \mathbf{A}_t \Delta x_{t|t} + \mathbf{B}_t \Delta \mathbf{u}_{t,j} + \mathbf{E}_t \mathbf{w}_t \quad \{\textit{Stacked EV Predictions}\}$$

$$\mathbf{A}_t = \begin{bmatrix} I_4 \\ A_{t|t} \\ \vdots \\ \prod_{k=t}^{t+N-1} A_{k|t} \end{bmatrix}$$

$$\mathbf{B}_t = \begin{bmatrix} O & \cdots & \cdots & O \\ B_{t|t} & O & \cdots & O \\ \vdots & \ddots & \ddots & \vdots \\ \prod_{k=t+1}^{t+N-1} A_{k|t} B_{t|t} & \cdots & \cdots & B_{t+N-1|t} \end{bmatrix}$$

$$\mathbf{E}_t = \begin{bmatrix} O & \cdots & \cdots & O \\ I_4 & O & \cdots & O \\ A_{t+1|t} & I_4 & \cdots & O \\ \vdots & \ddots & \ddots & \vdots \\ \prod_{k=t+1}^{t+N-1} A_{k|t} & \cdots & \cdots & I_4 \end{bmatrix} \tag{25}$$

$$\Delta \mathbf{o}_{t,j} = \mathbf{T}_t^j o_{t|t} + \mathbf{C}_t^j + \mathbf{F}_t^j \mathbf{n}_{t,j} \quad \{\textit{Stacked TV Predictions}\}$$

$$\mathbf{T}_t^j = \begin{bmatrix} I_2 \\ T_{t|t,j} \\ T_{t+1|t,j} T_{t|t,j} \\ \vdots \\ \prod_{k=t}^{t+N-1} T_{k|t,j} \end{bmatrix}$$

$$\mathbf{C}_t^j = \begin{bmatrix} O \\ c_{t|t,j} \\ c_{t+1|t,j} + T_{t+1|t,j} c_{t|t,j} \\ \vdots \\ c_{t+N-1|t,j} + \sum_{k=t}^{t+N-1} \prod_{l=k+1}^{t+N-1} T_{l|t,j} c_{k|t,j} \end{bmatrix}$$

$$\mathbf{L}_t^j = \begin{bmatrix} O & \cdots & \cdots & O \\ I_2 & O & \cdots & O \\ T_{t+1|t,j} & I_2 & \cdots & O \\ \vdots & \ddots & \ddots & \vdots \\ \prod_{k=t+1}^{t+N-1} T_{k|t,j} & \cdots & \cdots & I_2 \end{bmatrix} \tag{26}$$

$$\boldsymbol{\Sigma}_w = I_N \otimes \Sigma_w, \quad \boldsymbol{\Sigma}_n^j = \text{blkdiag}(\Sigma_{t|t,j}, \ldots, \Sigma_{t+N-1|t,j}) \tag{27}$$

$$\mathbf{Q} = I_{N+1} \otimes Q, \ \mathbf{R} = I_N \otimes R. \tag{28}$$

REFERENCES

[1] N. H. T. S. Admin. (2020). *Automated Vehicles for Safety*. [Online]. Available: https://www.nhtsa.gov/technology-innovation/automated-vehicles-safety

[2] M. Company. (2023). *Autonomous Driving's Future: Convenient and Connected*. [Online]. Available: https://www.mckinsey.com/industries/automotive-and-assembly/our-insights/autonomous-drivings-future-convenient-and-connected

[3] H. Chae, Y. Jeong, H. Lee, J. Park, and K. Yi, "Design and implementation of human driving data–based active lane change control for autonomous vehicles," *Proc. Inst. Mech. Engineers, Part D, J. Automobile Eng.*, vol. 235, no. 1, pp. 55–77, Jan. 2021.

[4] X. Zhang, A. Liniger, A. Sakai, and F. Borrelli, "Autonomous parking using optimization-based collision avoidance," in *Proc. IEEE Conf. Decis. Control (CDC)*, Dec. 2018, pp. 4327–4332.

[5] N. H. T. S. Admin. (2010). *Crash Factors in Intersection-related Crashes: An On-scene Perspective*. [Online]. Available: http://www-nrd.nhtsa.dot.gov/Pubs/811366.pdf

[6] L. Wei, Z. Li, J. Gong, C. Gong, and J. Li, "Autonomous driving strategies at intersections: Scenarios, state-of-the-art, and future outlooks," 2021, *arXiv:2106.13052*.

[7] H. A. P. Blom and Y. Bar-Shalom, "The interacting multiple model algorithm for systems with Markovian switching coefficients," *IEEE Trans. Autom. Control*, vols. AC-33, no. 8, pp. 780–783, Aug. 1988.

[8] Y. Chai, B. Sapp, M. Bansal, and D. Anguelov, "MultiPath: Multiple probabilistic anchor trajectory hypotheses for behavior prediction," 2019, *arXiv:1910.05449*.

[9] T. Salzmann, B. Ivanovic, P. Chakravarty, and M. Pavone, "Trajectron++: Dynamically-feasible trajectory forecasting with heterogeneous data," in *Proc. Eur. Conf. Comput. Vis.*, Aug. 2020, pp. 683–700.

[10] I. Batkovic, U. Rosolia, M. Zanon, and P. Falcone, "A robust scenario MPC approach for uncertain multi-modal obstacles," *IEEE Control Syst. Lett.*, vol. 5, no. 3, pp. 947–952, Jul. 2021.

[11] Y. Chen, U. Rosolia, W. Ubellacker, N. Csomay-Shanklin, and A. D. Ames, "Interactive multi-modal motion planning with branch model predictive control," *IEEE Robot. Autom. Lett.*, vol. 7, no. 2, pp. 5365–5372, Apr. 2022.

[12] S. H. Nair, V. Govindarajan, T. Lin, C. Meissen, H. E. Tseng, and F. Borrelli, "Stochastic MPC with multi-modal predictions for traffic intersections," in *Proc. IEEE 25th Int. Conf. Intell. Transp. Syst. (ITSC)*, Oct. 2022, pp. 635–640.

[13] T. Li, L. Zhang, S. Liu, and S. Shen, "MARC: Multipolicy and risk-aware contingency planning for autonomous driving," *IEEE Robot. Autom. Lett.*, vol. 8, no. 10, pp. 6587–6594, Oct. 2023.

[14] Z. Huang, P. Karkus, B. Ivanovic, Y. Chen, M. Pavone, and C. Lv, "DTPP: Differentiable joint conditional prediction and cost evaluation for tree policy planning in autonomous driving," 2023, *arXiv:2310.05885*.

[15] W. Schwarting, J. Alonso-Mora, and D. Rus, "Planning and decision-making for autonomous vehicles," *Annu. Rev. Control, Robot., Auto. Syst.*, vol. 1, no. 1, pp. 187–210, 2018.

[16] T. Brüdigam, M. Olbrich, D. Wollherr, and M. Leibold, "Stochastic model predictive control with a safety guarantee for automated driving," *IEEE Trans. Intell. Vehicles*, vol. 8, no. 1, pp. 22–36, Jan. 2023.

[17] U. Rosolia, X. Zhang, and F. Borrelli, "Data-driven predictive control for autonomous systems," *Annu. Rev. Control, Robot., Auto. Syst.*, vol. 1, no. 1, pp. 259–286, May 2018.

[18] A. Mesbah, "Stochastic model predictive control: An overview and perspectives for future research," *IEEE Control Syst. Mag.*, vol. 36, no. 6, pp. 30–44, Dec. 2016.

[19] A. Carvalho, Y. Gao, S. Lefevre, and F. Borrelli, "Stochastic predictive control of autonomous vehicles in uncertain environments," in *Proc. Int. Symp. Adv. Vehicle Control*, Tokyo, Japan, Sep. 2014, pp. 712–719.

[20] A. Gray, Y. Gao, T. Lin, J. K. Hedrick, and F. Borrelli, "Stochastic predictive control for semi-autonomous vehicles with an uncertain driver model," in *Proc. 16th Int. IEEE Conf. Intell. Transp. Syst. (ITSC)*, Oct. 2013, pp. 2329–2334, doi: 10.1109/ITSC.2013.6728575.

[21] D. Moser, R. Schmied, H. Waschl, and L. D. Re, "Flexible spacing adaptive cruise control using stochastic model predictive control," *IEEE Trans. Control Syst. Technol.*, vol. 26, no. 1, pp. 114–127, Jan. 2018.

[22] V. Causevic, Y. Fanger, T. Brüdigam, and S. Hirche, "Information-constrained model predictive control with application to vehicle platooning," *IFAC-PapersOnLine*, vol. 53, no. 2, pp. 3124–3130, 2020.

[23] T. Brüdigam, A. Capone, S. Hirche, D. Wollherr, and M. Leibold, "Gaussian process-based stochastic model predictive control for overtaking in autonomous racing," 2021, *arXiv:2105.12236*.

[24] G. C. Calafiore and M. C. Campi, "The scenario approach to robust control design," *IEEE Trans. Autom. Control*, vol. 51, no. 5, pp. 742–753, May 2006.

[25] O. de Groot, B. Brito, L. Ferranti, D. Gavrila, and J. Alonso-Mora, "Scenario-based trajectory optimization in uncertain dynamic environments," *IEEE Robot. Autom. Lett.*, vol. 6, no. 3, pp. 5389–5396, Jul. 2021.

[26] S. X. Wei, A. Dixit, S. Tomar, and J. W. Burdick, "Moving obstacle avoidance: A data-driven risk-aware approach," *IEEE Control Syst. Lett.*, vol. 7, pp. 289–294, 2023.

[27] S. H. Nair, E. H. Tseng, and F. Borrelli, "Collision avoidance for dynamic obstacles with uncertain predictions using model predictive control," in *Proc. IEEE 61st Conf. Decis. Control (CDC)*, Jun. 2022, pp. 5267–5272.

[28] M. Schuurmans, A. Katriniok, C. Meissen, H. E. Tseng, and P. Patrinos, "Safe, learning-based MPC for highway driving under lane-change uncertainty: A distributionally robust approach," *Artif. Intell.*, vol. 320, Jul. 2023, Art. no. 103920.

[29] B. Zhou, W. Schwarting, D. Rus, and J. Alonso-Mora, "Joint multi-policy behavior estimation and receding-horizon trajectory planning for automated urban driving," in *Proc. IEEE Int. Conf. Robot. Autom. (ICRA)*, May 2018, pp. 2388–2394.

[30] A. Wang, A. Jasour, and B. C. Williams, "Non-Gaussian chance-constrained trajectory planning for autonomous vehicles under agent uncertainty," *IEEE Robot. Autom. Lett.*, vol. 5, no. 4, pp. 6041–6048, Oct. 2020.

[31] K. Ren, H. Ahn, and M. Kamgarpour, "Chance-constrained trajectory planning with multimodal environmental uncertainty," *IEEE Control Syst. Lett.*, vol. 7, pp. 13–18, 2023.

[32] S. H. Nair, V. Govindarajan, T. Lin, Y. Wang, E. H. Tseng, and F. Borrelli, "Stochastic MPC with dual control for autonomous driving with multi-modal interaction-aware predictions," 2022, *arXiv:2208.03525*.

[33] J. Zhou, B. Olofsson, and E. Frisk, "Interaction-aware motion planning for autonomous vehicles with multi-modal obstacle uncertainty predictions," *IEEE Trans. Intell. Vehicles*, vol. 9, no. 1, pp. 1305–1319, Jan. 2024.

[34] R. Oliveira, S. H. Nair, and B. Wahlberg, "Interaction and decision making-aware motion planning using branch model predictive control," 2023, *arXiv:2302.00060*.

[35] M. Ono and B. C. Williams, "Iterative risk allocation: A new approach to robust model predictive control with a joint chance constraint," in *Proc. 47th IEEE Conf. Decis. Control*, Dec. 2008, pp. 3427–3432.

[36] V. Sivaramakrishnan, A. P. Vinod, and M. M. K. Oishi, "Convexified open-loop stochastic optimal control for linear non-Gaussian systems," 2020, *arXiv:2010.02101*.

[37] K. Liu, N. Li, H. E. Tseng, I. Kolmanovsky, and A. Girard, "Interaction-aware trajectory prediction and planning for autonomous vehicles in forced merge scenarios," *IEEE Trans. Intell. Transp. Syst.*, vol. 24, no. 1, pp. 474–488, Jan. 2023.

[38] J. Ma, F. Zhou, Z. Huang, C. L. Melson, R. James, and X. Zhang, "Hardware-in-the-loop testing of connected and automated vehicle applications: A use case for queue-aware signalized intersection approach and departure," *Transp. Res. Rec., J. Transp. Res. Board*, vol. 2672, no. 22, pp. 36–46, Dec. 2018.

[39] T. Tettamanti, M. Szalai, S. Vass, and V. Tihanyi, "Vehicle-in-the-loop test environment for autonomous driving with microscopic traffic simulation," in *Proc. IEEE Int. Conf. Veh. Electron. Saf. (ICVES)*, Sep. 2018, pp. 1–6.

[40] T. Ard, L. Guo, J. Han, Y. Jia, A. Vahidi, and D. Karbowski, "Energy-efficient driving in connected corridors via minimum principle control: Vehicle-in-the-loop experimental verification in mixed fleets," *IEEE Trans. Intell. Vehicles*, vol. 8, no. 2, pp. 1279–1291, Feb. 2023.

[41] E. Joa, H. Lee, E. Yongkeun Choi, and F. Borrelli, "Energy-efficient lane changes planning and control for connected autonomous vehicles on urban roads," 2023, *arXiv:2304.08576*.

[42] T. Fork, H. E. Tseng, and F. Borrelli, "Models and predictive control for nonplanar vehicle navigation," in *Proc. IEEE Int. Intell. Transp. Syst. Conf. (ITSC)*, Sep. 2021, pp. 749–754.

[43] J. Houston et al., "One thousand and one hours: Self-driving motion prediction dataset," in *Proc. Conf. Robot. Learn.*, 2020, pp. 1–22.

[44] H. Caesar et al., "NuScenes: A multimodal dataset for autonomous driving," 2019, *arXiv:1903.11027*.

[45] F. Borrelli, A. Bemporad, and M. Morari, *Predictive Control for Linear and Hybrid Systems*. Cambridge, U.K.: Cambridge Univ. Press, 2017.
[46] P. J. Goulart, E. C. Kerrigan, and J. M. Maciejowski, "Optimization over state feedback policies for robust control with constraints," *Automatica*, vol. 42, no. 4, pp. 523–533, Apr. 2006.
[47] D. Kuhn, P. M. Esfahani, V. A. Nguyen, and S. Shafieezadeh-Abadeh, "Wasserstein distributionally robust optimization: Theory and applications in machine learning," in *Operations Research Management Science in the Age of Analytics*. Catonsville, MD, USA: Informs, 2019, pp. 130–166.
[48] A. Dosovitskiy, G. Ros, F. Codevilla, A. Lopez, and V. Koltun, "CARLA: An open urban driving simulator," in *Proc. 1st Annu. Conf. Robot Learn.*, vol. 78, 2017, pp. 1–16.
[49] A. Wächter and L. T. Biegler, "On the implementation of an interior-point filter line-search algorithm for large-scale nonlinear programming," *Math. Program.*, vol. 106, no. 1, pp. 25–57, Mar. 2006.
[50] Gurobi Optim., LLC. (2021). *Gurobi Optimizer Reference Manual*. [Online]. Available: https://www.gurobi.com

Siddharth H. Nair received the B.Tech. and M.Tech. degrees in aerospace engineering from Indian Institute of Technology at Bombay, Bombay, India, in 2018, with a minor in systems and control engineering, and the Ph.D. degree in mechanical engineering from the University of California, Berkeley, CA, USA, in 2024, with a focus on control, optimization, and machine learning.

His research interests include data-driven nonlinear predictive control, motion planning in uncertain environments, and machine learning for numerical optimal control.

Hotae Lee (Member, IEEE) received the B.S. degree in mechanical engineering from Seoul National University, Seoul, South Korea, in 2018. He is currently pursuing the Ph.D. degree in mechanical engineering with the University of California at Berkeley, Berkeley, CA, USA.

His research interests include stochastic model predictive control, optimization and machine learning for motion planning under uncertainties, and practical robotics/automation applications.

Eunhyek Joa (Member, IEEE) received the B.S. and M.S. degrees in mechanical engineering from Seoul National University, Seoul, South Korea, in 2014 and 2016, respectively. He is currently pursuing the Ph.D. degree in mechanical engineering with the University of California at Berkeley, Berkeley, CA, USA, sponsored by Korean Government Scholarship Program.

He was a Research Engineer with the Institute of Advanced Machines and Design, Seoul National University, from 2016 to 2020. His research interests include data-driven control, constrained optimal control, and model predictive control and their applications to advanced automotive control.

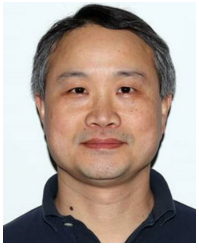

Yan Wang received the B.S. degree in mechanical engineering and the M.S. degree in mechatronics from Tsinghua University, Beijing, China, in 1994 and 1997, respectively, and the Ph.D. degree in mechanical engineering from the University of California at Santa Barbara, Santa Barbara, CA, USA, in 2001, focusing on controls.

He has since been with Ford Research and Advanced Engineering working on different control problems. He accumulated more than 15 years of experience in actuator design and mechatronics controls, with interdisciplinary background in mechanical, electrical, and magnetic systems. He then moved to the field of adaptive and optimal control for automotive applications, focusing on automotive calibration and optimal/adaptive control problems. His main research interests include the application and realtime implementation of advanced/modern control methods, including robust control, adaptive control, system identification, optimal control, model predictive control, and data analytics and machine learning, on vehicle design, control, and calibration. His recent interests include adaptive DOE, AI/ML in system ID and adaptation, real-time optimization, sensor fusion and diagnostics, and predictive optimization with preview.

H. Eric Tseng received the B.S. degree from National Taiwan University, Taipei, Taiwan, in 1986, and the M.S. and Ph.D. degrees in mechanical engineering from the University of California at Berkeley, Berkeley, CA, USA, in 1991 and 1994, respectively.

In 1994, he joined Ford Motor Company, Dearborn, MI, USA. At Ford, he had a productive career and retired as a Senior Technical Leader of the Controls and Automated Systems in Research and Advanced Engineering, from 1994 to 2022. He is currently a Distinguished University Professor with The University of Texas at Arlington, Arlington, TX, USA. Many of his contributed technologies led to production vehicles implementation. He has over 100 U.S. patents and over 160 publications.

Dr. Tseng is a member of the National Academy of Engineering in 2021. His technical achievements have been honored with the Ford's Annual Technology Award, the Henry Ford Technology Award, on seven occasions. Additionally, he was a recipient of the Control Engineering Practice Award from American Automatic Control Council in 2013 and that of Sochiro Honda Medal from American Society of Mechanical Engineers in 2024.

Francesco Borrelli (Fellow, IEEE) received the Laurea degree in computer science engineering from the University of Naples Federico II, Naples, Italy, in 1998, and the Ph.D. degree from ETH Zürich, Zürich, Switzerland, in 2002.

He is currently a Professor with the Department of Mechanical Engineering, University of California at Berkeley, Berkeley, CA, USA. He is the author of more than 100 publications in the field of predictive control and the author of the book *Constrained Optimal Control of Linear and Hybrid Systems* (Springer Verlag). His research interests include constrained optimal control, model predictive control, and its application to advanced automotive control and energy-efficient building operation.

Dr. Borrelli was a recipient of the 2009 National Science Foundation CAREER Award and the 2012 IEEE Control System Technology Award. In 2008, he was appointed as the Chair of the IEEE Technical Committee on Automotive Control.